JOURNAL OF GEOPHYSICAL RESEARCH, VOL. 93, NO. C12, PAGES 15,561–15,584, DECEMBER 15, 1988

Atmospheric Conditions During the Spring and Fall Transitions in the Coastal Ocean Off Western United States

P. TED STRUB AND CORINNE JAMES

College of Oceanography, Oregon State University, Corvallis

We examine large-scale atmospheric behavior around the time of the spring and fall transitions in the coastal ocean off the west coast of North America. Records of adjusted sea level (ASL), coastal wind stress, sea level atmospheric pressure (SLP), and 500-mbar heights for the years 1971–1975 and 1980–1983 are analyzed. The records cover periods of 91 days, centered on the dates of the spring and fall transitions as determined from coastal adjusted sea level data. Empirical orthogonal functions are obtained from the ASL, coastal wind stress, and SLP records. The two dominant modes of the ASL and coastal wind stress are similar around the times of both the spring and fall transitions, and the time series for these modes are highly correlated with one another. Transitionlike behavior is evident in the time series of the first modes in both spring and fall, but the spring transition is more pronounced. Principal estimator patterns, formed from the dominant empirical orthogonal functions show the spatial patterns of SLP which force the ASL and coastal wind stress during the transitions. The SLP pattern which coincides with the spring transition is the formation of a high-pressure system centered at 45°N and 140°W along with the development of a low-pressure cell over the southwest continental United States. Inspection of the 500-mbar height composites for 91 days surrounding the spring transition for the 9 years reveals the formation of a ridging pattern and diffluent flow over the western United States at the time of the transition; following the transition, the ridging relaxes but the diffluent flow over the continent remains for the duration of the 45 days examined here. The fall transition is characterized by a rise in ASL, particularly north of 40°N, and a change from southward to northward wind stress. The SLP pattern which coincides with the fall transition involves the appearance of a low-pressure system off western North America centered at 50°N and 140°W, representing the passage of synoptic storms through the region. Prior to the fall transition, the 500-mbar heights are somewhat diffluent and show a trough over the southwestern United States; after the transition the 500-mbar flow over the northeast Pacific and North America is nearly zonal.

1. Introduction and Background

The purpose of this paper is to explore the mean structure of the large-scale atmospheric events which force the spring and fall transitions in the coastal ocean off the west coast of North America. The term "spring transition" is used here to denote the sudden onset of the spring/summer upwelling regime in the coastal ocean. The "fall transition" is the reverse process, that is, the onset of the fall/winter downwelling regime.

The spring transition typically occurs over the period of a week [*Huyer et al.*, 1979; *Breaker and Mooers*, 1986; *Lentz*, 1987; *Wickham et al.*, 1987; *Strub et al.*, 1987*a*]. During the transition, coastal sea levels drop, alongshore surface currents become southward, and surface temperatures decrease due to the onset or increase in the strength of upwelling. The low sea level and southward current appear to be persistent off central Oregon but more intermittent off California [*Strub et al.*, 1987*a*, *b*] (hereinafter referred to as S1 and S2). North of approximately 38°N the onset of the transition is coincident with a several day period of strong, southward winds, and the transition in that region is generally thought to be a wind-forced event. The connection between southward winds and upwelling is less convincing south of approximately 38°N, where the sudden transition is not seen in some years [S1; *Breaker and Mooers*, 1986; *Wickham et al.*, 1987], and the response of the ocean appears more short-lived than the southward wind [*Brink et al.*, 1984]. Flow off southern California is thought by some to be affected by deep water currents, such as onshore meanders of the California Current, making the response to the local wind a less dominant component of the flow [*Hickey*, 1979; *Hickey and Pola*, 1983; *Wickham et al.*, 1987]. Another factor that may affect the spring transition is the influence of propagating coastally trapped waves, indicated by the apparent northward progression of the spring transition during some years [S1; *Breaker and Mooers*, 1986]. Finally, *Werner and Hickey* [1983] suggest that the southward alongshore pressure gradient which opposes the northward wind in winter acts in concert with the sudden onset of southward winds after the spring transition to produce a response in the ocean that appears stronger than the wind forcing.

Although the fall transition has not been as well studied as the spring transition, results from 1980 off Oregon suggest a gradual transition in coastal ocean conditions over several months [*Reid*, 1987] rather than the week-long transition seen in spring. A more gradual fall transition is also suggested by *Wickham et al.* [1987] using data from 1978–1980 off central California and by S1 using data from 1981–1982 off California and southern Oregon. The driving mechanism for the fall transition is presumed to be a sequence of storms, typically beginning in September with greater wind stress in the north [*Reid*, 1987]. Hickey [1989] points out that the seasonal growth of the poleward undercurrent over the upper slope reaches a maximum in late summer off Washington when poleward flow also occurs over the shelf. Thus the return to conditions similar to fall and winter in the coastal ocean may begin independently of the local wind.

S1 used 9 years of sea level and wind stress data from six stations covering the region between 33.7°N and 48.5°N to

Paper number 88JC03498.
0148-0227/88/88JC-03498$05.00

show the nature of the alongshore wind and sea level during a composite spring transition. Their method was to estimate the date of the transition from the sudden and persistent drop in sea level at Crescent City (41.8°N) on each of the 9 years of available sea level data. Designating this date as day 16 in a 30-day record for each year, they ensemble averaged the sea level and alongshore wind stress records from the 9 years to form composite 30-day records representing an "average" spring transition at the six stations. The results showed the large-scale (in the alongshore direction) extent of the sea level event, with a northward progression of the signal, and the coincident southward wind stress event. The region of strong forcing and response covered northern California, Oregon, and Washington. The response was less strong off southern and central California.

A number of the oceanographers who have studied the spring transition link the increase in southward winds at coastal stations during the transition to a rapid increase in the size and the strength of the subtropical high-pressure system in the eastern north Pacific. Very little documentation can be found in the atmospheric literature to support this abrupt, large-scale seasonal change. Such repeatable, sudden transitions belong to a class of phenomena called "singularities" by meteorologists and have a long (and at times controversial) history in the climatological literature [*Lanzante*, 1983]. *Fleming et al.* [1987] looked for sudden shifts in the zonally averaged position of the 500 mbar jet on a yearly basis and found no evidence for "abrupt and monotonic" latitudinal shifts in position. The use of zonal averages prevented this analysis from seeing shifts that occur in one location only. S1 and *Lentz* [1987] refer to reports by *Lahey et al.* [1958] and *Bryson and Lahey* [1958] in which surface pressure data from the early 20th century were averaged by calendar day to produce 5-day mean pressure maps covering the annual cycle. Lentz reproduced a graph from Bryson and Lahey showing the position of the Aleutian low as a function of time, supporting the contention that the Aleutian low weakens and splits into two smaller low-pressure systems over Asia and the Bering Sea at the beginning of April. *Lanzante* [1983] used a 30-year (1947–1976) time series of 700-mbar heights over the North Pacific Ocean, North America, and the North Atlantic Ocean to look for singularities during all seasons at different locations. He mentions a spring transition of increasing 700-mbar heights over the central North Pacific Ocean, but this transition is spread over the period from early March to June. Lanzante averages the years together by calendar day and acknowledges the fact that this method smooths sudden transitions which vary in date between years. Following S1, the present analysis avoids this by centering the atmospheric records for each year around the date of the transition as determined from the sea level records.

2. DATA

The oceanographic data used in this study are the same 9 years of sea level data used by S1. Hourly tide gauge data were available from six locations from approximately 34°N to 48°N for 1971–1975 and 1980–1983. The locations are Los Angeles (LA) at 33.7°N, Monterey (MO) at 36.6°N, San Francisco (SF) at 37.8°N, Crescent City (CC) at 41.8°N, South Beach (SB) at 44.6°N, and Neah Bay (NB) at 48.4°N. Atmospheric pressures were added to the sea levels to produce records of adjusted sea level (ASL). These records were low-pass filtered (half power at 46 hours) to eliminate tides and the diurnal cycle and decimated to daily values. A linear trend, caused mostly by changing tide gauge elevations, was removed from each complete 1971–1975 and 1980–1983 record. The period covered by these sea level data limits the analysis of atmospheric data to these 9 years.

Daily fields of sea level ressure (SLP) and surface winds were obtained from the Fleet Numerical Oceanography Center (FNOC) for the northern hemisphere on a grid with approximately 380-km resolution. These were interpolated to a 5° grid. The pressure fields are calculated by FNOC from a "blend" of pressure and wind observations [*Mendenhall et al.*, 1977]. The FNOC winds are calculated geostrophically by FNOC from the pressure fields, then reduced in magnitude and rotated according to a variable boundary-layer parameterization [*Mihok and Kaitala*, 1976]. We converted wind components to wind stress using a constant drag coefficient of 1.3×10^{-3}. These wind stresses were interpolated to the six tide gauge locations, and the principal axes of the wind stress were found. Previous studies have found measured winds to be strongly polarized in the alongshore direction; winds derived from atmospheric pressure fields are less strongly polarized but enough so that the component along their major axis is most closely correlated with the alongshore component of the measured wind [*Halliwell and Allen*, 1987]. In this study the component along the major axis at each tide gauge location is used to represent the coastal, alongshore wind stress. Daily 500-mbar heights from the National Meteorological Center were also obtained and interpolated to the same 5° grid as the SLP and FNOC winds.

3. METHODS

Sea level data from Crescent City were used to define the date of the spring transitions for each of 9 years by S1. These same dates for the spring transitions are used here. Sea level data from South Beach were used to define the date of the fall transition, since the transition appears more clearly in the northern locations. In general, the dates of the transitions correspond to the time when the sea level changes sign and stays positive or negative for more than 10 days. Some subjectivity is involved in picking these dates; sea levels from neighboring stations were examined to confirm the transition date. The transition dates were made the midpoints of 91-day records of the various data. The 91-day records of sea level at Crescent City in spring and at South Beach in fall are shown in Figure 1. Composite transition events were formed by ensemble averaging the 9 yearly records to form one 91-day record, centered on the transition, for each type of data. The composite records were then averaged over periods of 5, 15, 30, and 45 days to show the seasonal progression over several time scales.

The statistical characteristics of the data were examined by combining the 91-day records for the individual years to form 819-day records for each type of data. Empirical orthogonal functions (EOFs) were found from these 819-day records. The time series associated with the spatial EOF functions were used to look at the correlations between the major patterns of variability in the data. Decorrelation time scales for each of the variables were formed by integrating their lagged autocorrelation functions (formed from the 91-day records). These time scales were mostly in the range of 1.5–3 days. A value of 3 days was chosen as a conservative estimate of the decorrela-

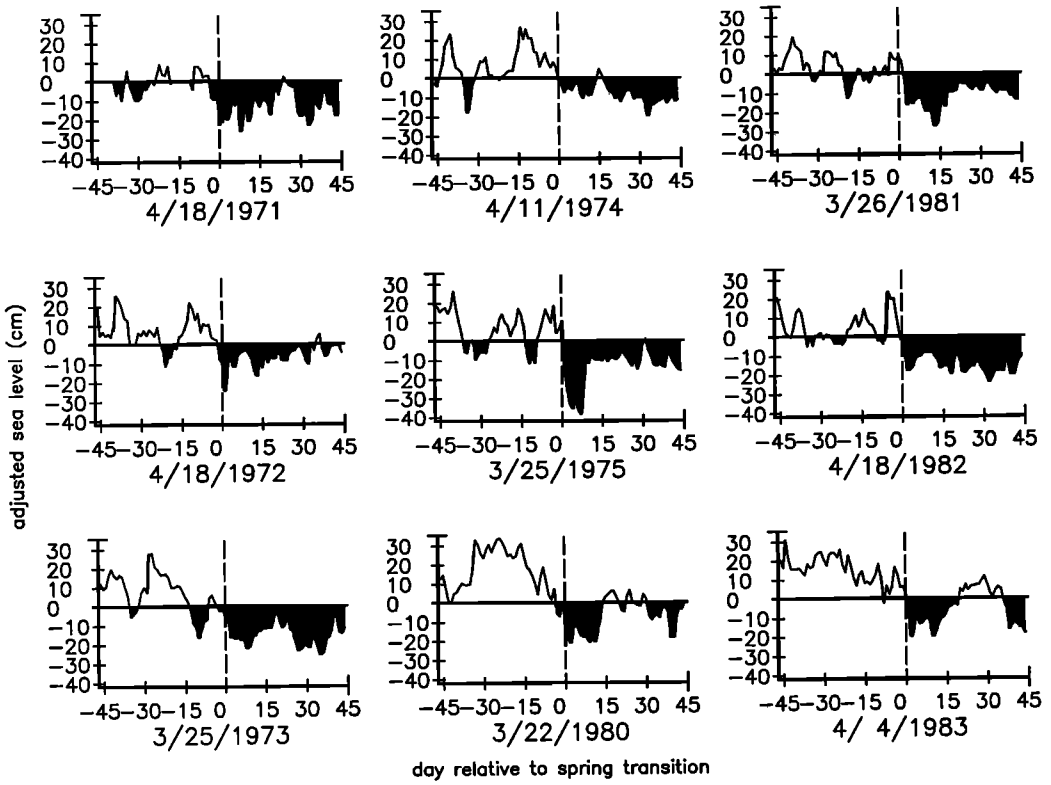

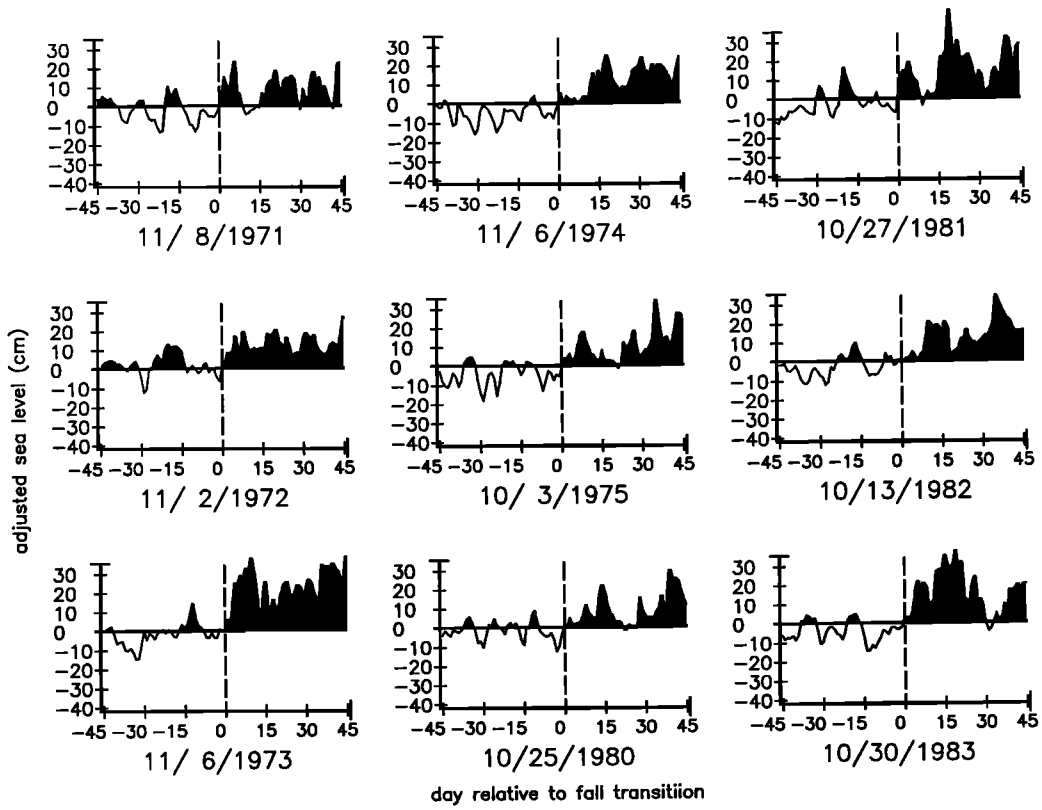

Fig. 1. Sea level for the 91-day periods surrounding the transition on each of the 9 years considered. A secular trend has been removed from the 1971–1975 and 1980–1983 records. The date of the transition (shown below each plot) is chosen and assigned to day 0 for each year. (*a*) Data from Crescent City during the spring transition; (*b*) data from South Beach during the fall transition.

tion time scale for all the variables. This value was used to determine the number of independent data points (degrees of freedom) in correlations between the variables.

Interpretation of the EOF analysis was straightforward for ASL and alongshore wind stress, but not for SLP. Although the examination of raw EOF patterns is a common practice in oceanography and meteorology, there are known problems associated with their use, as reviewed in detail by *Richman* [1986]. The basic problem is that each EOF tries to explain as much of the remaining variance in the entire domain as possible, regardless of its physical cause. The result is that each EOF mode may represent a mix of the dominant physical processes, as shown by *Richman* [1986]. Richman also presents examples of other problems such as domain shape dependence (the dominant EOFs for a region of a given geometry always look roughly the same in terms of the number and placement of zero crossings) and subdomain stability (breaking the region up into subdomains and finding EOFs results in a different pattern than when the whole region is analyzed at once).

Alternate methods of analyzing the EOFs usually involve forming new spatial patterns and time series from linear combinations of the raw EOFs; this is referred to as rotating the EOFs. *Richman* [1986] presents a variety of approaches to this technique. The most commonly used of these in meteorological and oceanographic applications is the "varimax" method, which maximizes the second moment of the variance explained by the different modes rather than maximizing the sum of the remaining variance explained by each mode. It tends to spread the total variance over the chosen number of modes and to localize (in space) the variance of any one mode. *Horel* [1981] used this method to extract patterns of 500-mbar covariability that looked like the expected teleconnection patterns over North America, whereas the raw EOFs did not resemble these patterns. When the varimax rotation was applied to EOFs of alongshore wind stress, ASL and SLP for the spring transition, the ASL and wind stress remained easy to interpret but the SLP was not much clearer. For the case where six modes were examined the time series and spatial pattern of one of the modes (the sixth) did resemble the pattern expected for the spring transition, but there was no justification for choosing this mode other than its resemblance to the expected pattern. When more or fewer than six modes were rotated, this apparent spring transition mode was lost.

The method of principal estimator patterns (PEP), also known as canonical correlation analysis [*Hotelling*, 1936], proved to be the most useful method of showing the connection between the SLP fields and coastal ASL or wind stress. This method has been used by *Davis* [1977, 1978] to relate EOFs of one variable to those of another for the purpose of forecasting. By forming correlations of the time series of the two sets of EOFs a new series of ordered pairs of spatial functions are found for the two variables, with a single time series associated with each pair of spatial functions (one spatial function for each variable). *Graham and White* [1988] use this method to relate patterns of wind stress, sea surface temperature, and model pycnocline depths during the El Niño. We use it similarly to find the spatial patterns of SLP that share common time series with patterns of ASL and alongshore wind stress, rather than using the method to predict one variable from another.

The seasonal cycle was not removed before forming the composites, EOFs, PEPs, or correlations. If an annual harmonic were removed, the idealized signature of the transitions would change from a square step function to a sawtooth function. Since the purpose of the investigation is to determine whether the seasonal cycle actually consists of a more steplike transition and to examine the persistence of the change in state, the seasonal cycle was retained. This results in artificially higher correlations between all variables, which should be kept in mind when interpreting the results.

4. RESULTS

4.1. *Seasonal Cycles of ASL—Context for the Transitions*

Figures showing the complete 9 years of sea level and alongshore wind stress data can be found in S1 (their Figure 2). The seasonal cycles for sea level, currents, water temperatures, and winds are presented and discussed in S2. Sea level serves as a fairly good proxy variable for temperature and alongshore currents in the coastal ocean, with high sea levels corresponding to northward currents and higher temperatures (and vice versa). In general, sea levels are high during the fall/winter downwelling season and low during the spring/summer upwelling season. The range in seasonal cycles is greatest in the north. The low sea levels associated with upwelling in the north lag those in the south by about a month on the seasonal time scale; the lag between south and north for the spring transition event is usually only several days.

The seasonal cycle forms the context for the spring and fall transitions and can be depicted by the first two EOFs of ASL. Spatial eigenfunctions and their annual mean time series (ensemble averaged over the 9 years) for the first two EOFs of coastal ASL are shown in Figure 2, calculated from the entire 9 years of sea level data. Over the annual period these two functions account for 91% of the total variance. The third and higher functions account for less than 4% each.

The first eigenfunction, accounting for 76% of the variance, describes a coincident drop (negative time series) or rise (positive time series) in sea level over the entire coastal domain. The maximum response is in the north, with 3 times the response at SB and NB as found in the south at LA. The time series for the first mode closely resembles the time series of sea level measured at the three northern stations. The annual cycle shows a drop of 20–30 cm in the north over the 2-month March–April period (days 60–120), during which the spring transition usually occurs (Figure 1*a*). Sea levels associated with this mode are lowest in May, rising gradually until the end of September (day 273). There are larger fluctuations in October and a rapid rise of 10–15 cm at the beginning of November around the time of the fall transition.

The second eigenfunction, accounting for 15% of the variance, describes opposing sea level motion in the south and north of the domain. Its time series is approximately 90° out of phase with that of the first EOF. The maximum in the time series between March and April results in lowering of sea levels in the south. In the north this function keeps sea levels high while the first EOF alone would result in lowering sea levels. The combination of first and second modes describes the early drop of sea levels in the south as southward winds become stronger there, while storms continue to hold sea levels high in the north. The second EOF decreases in mag-

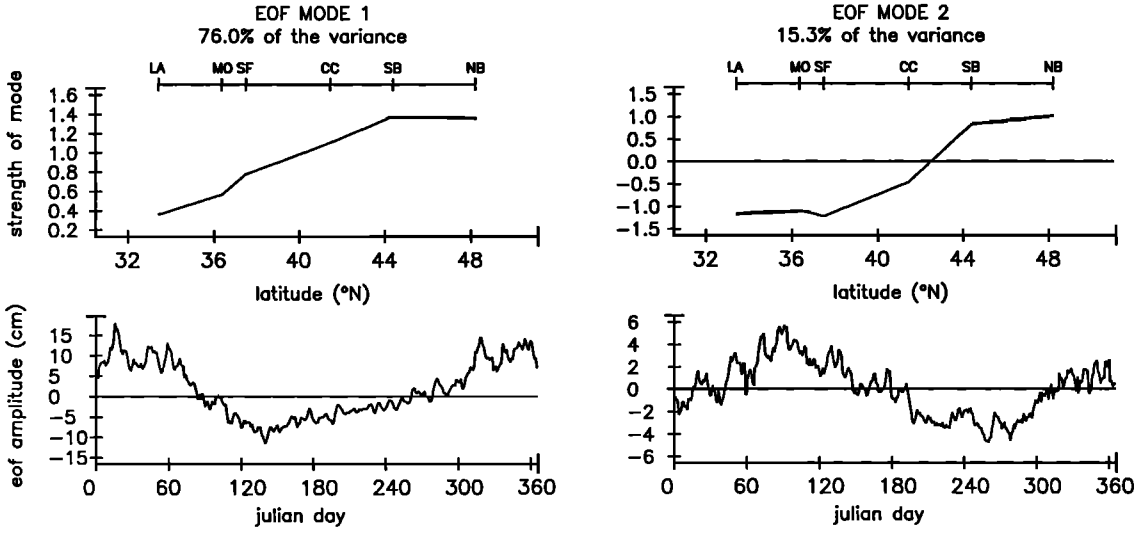

Fig. 2. The first two EOFs for the sea level from the six locations; these were calculated from the full 9 years of data. The spatial functions are shown in the top panels (tide gauge locations marked at the top). The 9-year averages of the time series of the EOF amplitudes are shown in the bottom panels, averaged by calendar day.

nitude in May–June, then reverses sign during July, concentrating the relative slope of the alongshore sea level (upward to the south) in the region between SB and SF. It becomes weakly positive when the first EOF becomes strongly positive, resulting in a rapid reversal of the relative sea level slope in November.

The averaging of the time series by calendar date smears the appearance of the transition and makes the seasonal cycle appear smooth. The seasonal cycle for the first EOF in Figure 2 looks similar (with its sign reversed) to the seasonal cycle of 700-mbar height over the Gulf of Alaska (60°N, 160°W) presented by *Lanzante* [1983]. In contrast, the abrupt nature of the spring transition can be seen in the first EOF time series from the individual years presented in Figure 3. The transition to negative values occurs rapidly on most years, although interannual variation is evident. The years 1973 and 1975 were

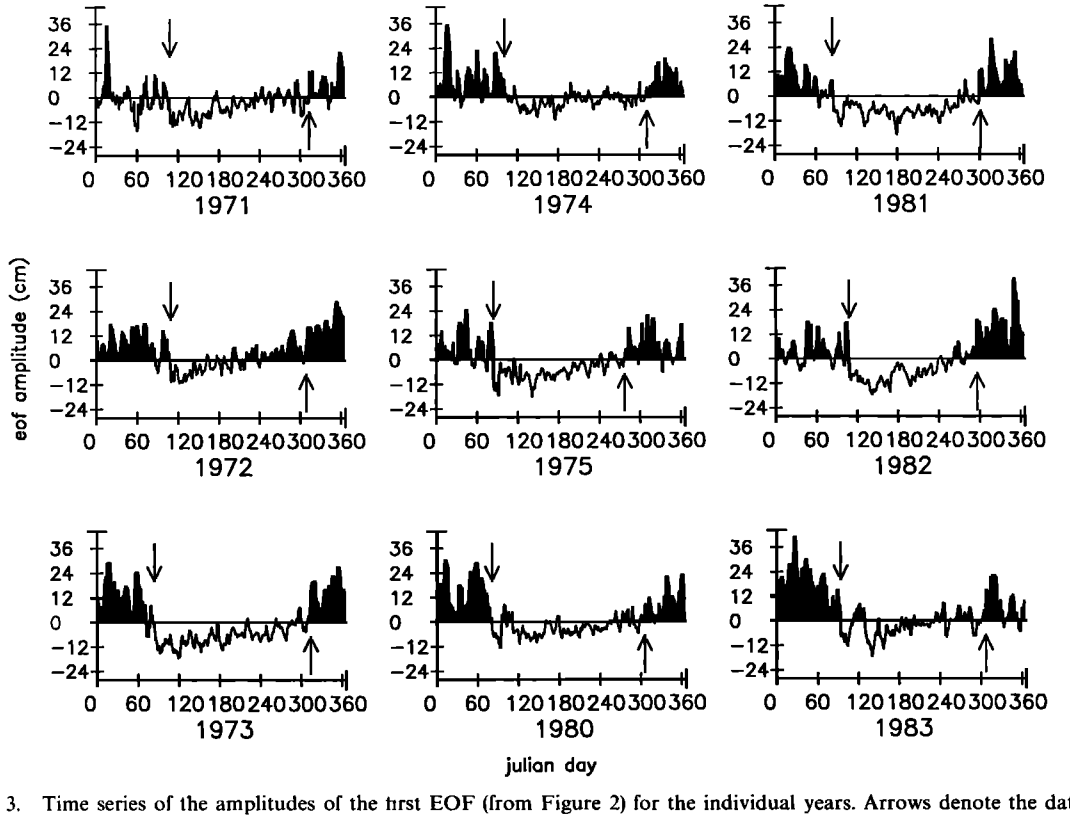

Fig. 3. Time series of the amplitudes of the first EOF (from Figure 2) for the individual years. Arrows denote the date chosen for the spring and fall transitions on each year.

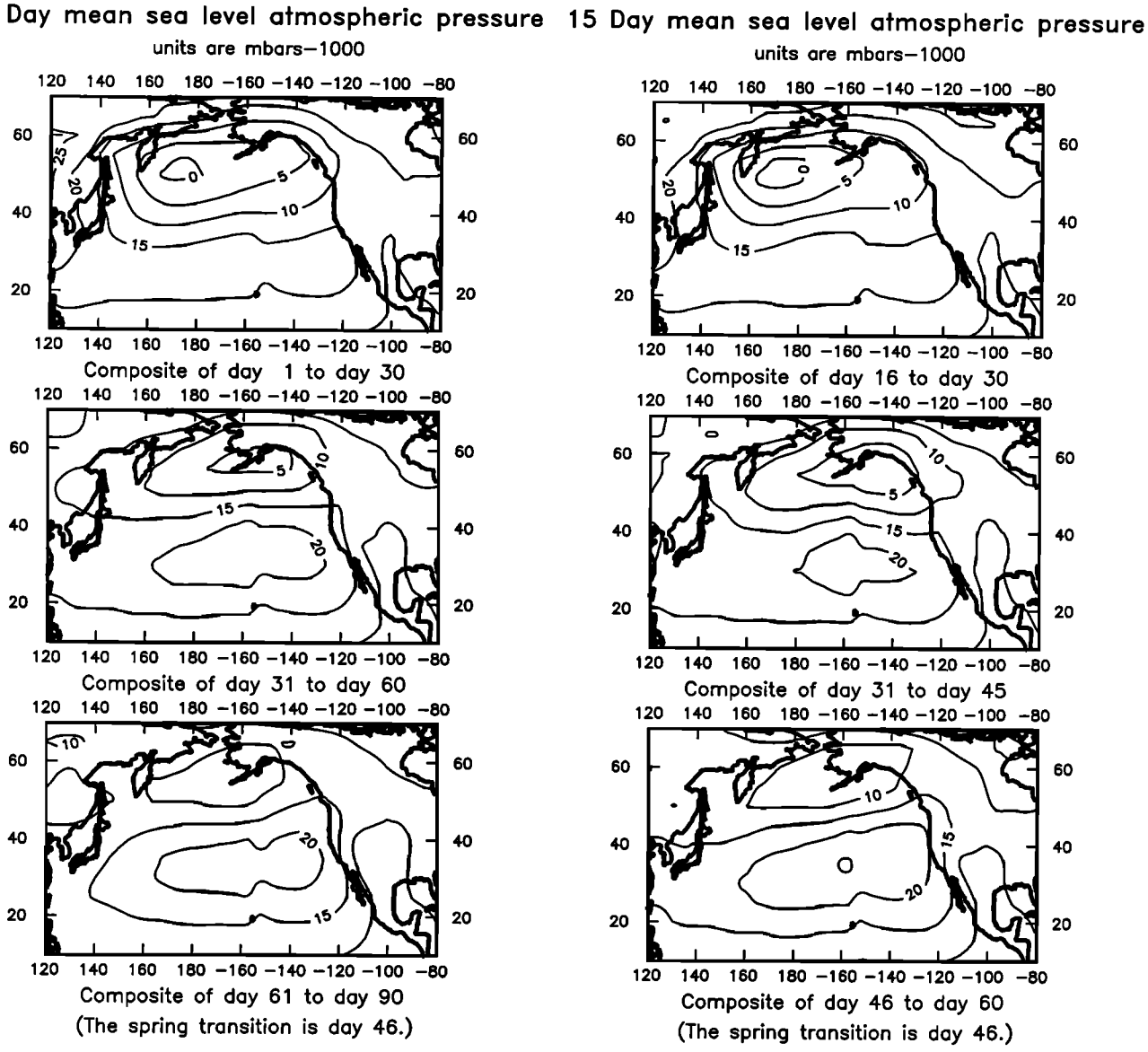

Fig. 4. Atmospheric fields from before and after the spring transition. Daily fields were composited for the 9 years; these were then averaged over 5, 15, 30, or 45 days. (*a*) Thirty-day means of SLP. Contours are for units of SLP in thousands of millibars. The transition occurs during the middle of the period covered by the center panel. (*b*) Fifteen-day means of SLP. The transition occurs between the periods covered by the center and bottom panels. (*c*) Five-day means of SLP. The transition occurs between the periods covered by the center and bottom panels. (*d*) Daily composites of SLP (note change in scale) for days 45, 47, and 49 (transition is day 46). (*e*) Daily composites of winds (same scale and days as in Figure 4*d*).

examined in detail by *Huyer et al.* [1979] in the original description of the spring transition off Oregon. These years have strong transitions, with long and persistent upwelling seasons, as does 1981. Other years show a strong transition with a shorter upwelling season, such as 1982, 1983, and 1972, or a long but weak upwelling season, such as 1980 and 1974; 1971 appears to have been in an intermittent upwelling mode for most of the winter, making the choice of transition date more subjective. A number of the years have a brief reversal (return to higher ASL for 5–15 days) after an initial spring transition event, which contributes to the subjective nature of the choice of date for the transition. The dates chosen for the spring transitions on each of the years using sea level at Crescent City are shown with downward arrows in Figure 3. The dates chosen for the fall transitions using sea level at South Beach are indicated by upward arrows.

4.2. *Spring Transition*

4.2.1. *Composite events in the atmosphere.* Figure 4*a* shows the 30-day averages of composite SLP, covering the 91-day spring transition period (contour labels show SLP minus 1000 mbar). The period for the middle panel is centered on the transition date, roughly the first week in April. The three panels can be interpreted as monthly means representing the late winter, early spring, and midspring. The seasonal cycle is as expected: the Aleutian low decreases in intensity and areal extent, splitting into weaker lows over Asia and the Aleutian Islands, while the subtropical high-pressure cell becomes evident during the month of the transition. Low pressure also strengthens and enlarges over the southern United States and Mexico. *Lentz* [1987] shows the climatological mean position of the Aleutian low [from *Bryson and Lahey*, 1958] to be 170°E, 50°N before April, splitting into separate

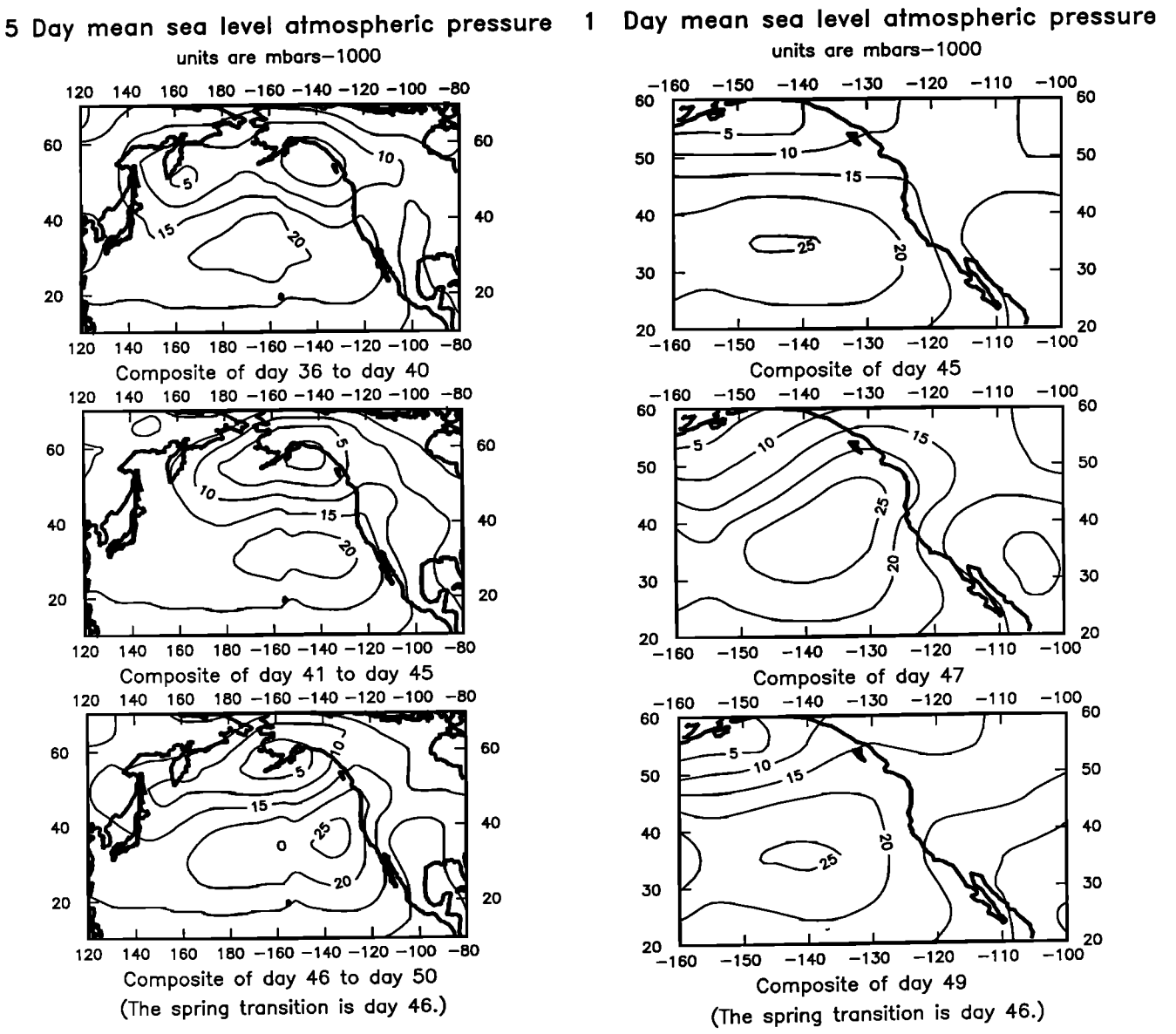

Fig. 4. (continued)

lows at around 60°N, 160°W and 50°N, 130°E. The positions of the low-pressure systems in our composites are in close agreement with the earlier studies, indicating that the ensemble mean of the 9 years of data used here is representative of the climatological mean.

Figure 4*b* shows 15-day averages of SLP for the two 15-day periods prior to the transition and for the period immediately following the transition. The cell of high pressure (>1020 mbar) appears in the 2 weeks before the transition. After the transition the high-pressure cell expands approximately 10° northward, that is, the region where the 1015-mbar contour crosses the coast moves from 40°N to above 50°N. The speed of the transition can be seen in the 5-day means shown in Figure 4*c*. The top two panels show the two 5-day periods prior to the transition, with little change in the position of the 1015-mbar contour. The expansion seen in these panels is accompanied by the strengthening of a meridionally elongated low-pressure cell over the southern United States and Mexico around 100°W, 20°–40°N. This region of low pressure (<1010 mbar) becomes continuous with the region of low pressure in the Gulf of Alaska just prior to the transition, and at the same time the Aleutian low strengthens. This may be the signature of a storm passing through the northwest just prior to the transition. The pattern evident in the bottom 5-day composite of Figure 4*c* remains fairly constant over the 45 days following the transition (not shown). In particular, the 1015-mbar isobar crossing the coast off British Columbia does not move south of 50°N after the transition in these 5-day composites, indicating the persistence of the high-pressure system.

Figures 4*a*–4*c* show that the intensification of the high-pressure system is concentrated in the region in the northeast Pacific between 20°–50°N and 120°–160°W. Figure 4*d* focuses on this region and shows the 1-day composites of SLP every other day for 3 days around the date of the transition. Daily composite wind fields for the same days are given in Figure 4*e*. These figures emphasize the rapid expansion of the high-pressure system over a several day period with steady alongshore winds of 10–15 m/s over a large region of coastal ocean.

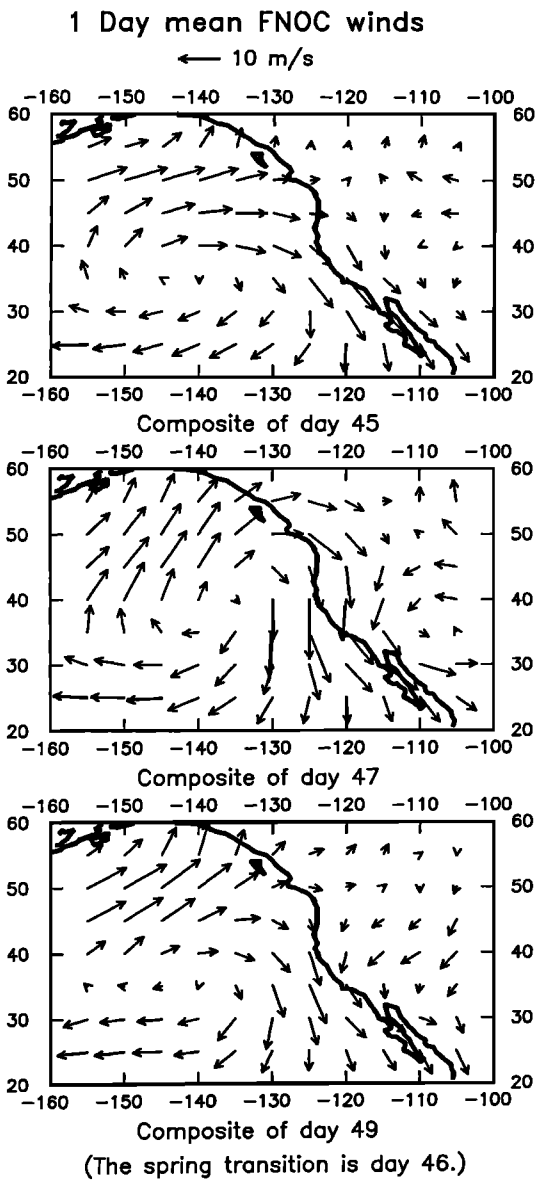

Fig. 4. (continued)

They also show the coincident deepening of a low-pressure system over the southwest.

Does the rapid change in atmospheric pressure at the surface correspond to a change in the upper atmospheric circulation? The seasonal progression of 500-mbar heights is seen in Figure 5, where 45-day averages of these composites are presented, covering the periods immediately before and after the transition. These correspond (roughly) to the picture seen in SLP in the top and bottom panels in Figure 4*a*. The flow is stronger prior to the transition and more zonal, especially south of 30°N. There is a trough in the western Pacific at the western edge of the figure, upstream of the center of the surface low pressure, and a ridge over western North America. The major changes after the transition are the northward movement and spreading of the contours over North America, the movement of the trough from the northwest to the northeast Pacific, and the development of a trough over the west coast of the United States south of 40°N. The troughs in the northeast Pacific and over the continent correspond to surface low pressures seen in Figure 4*a*. The development of the region of low pressure over the continent is coincident with the development of a diffluent flow over western North America (the term "diffluent flow" is used hereinafter to indicate the region of divergent streamlines where the 500-mbar jet spreads out and decelerates, as seen over the western United States at the bottom of Figure 5).

Figure 6 shows 5-day averages of 500 mbar heights covering the period from 10 days before to 5 days after the transition, the same periods for which SLP is shown in Figure 4*c*. The striking feature is the development of a ridge and trough pattern centered over the regions of surface high and low pressure. This is similar, in some respects, to the atmospheric blocking pattern which occurs periodically over the North Pacific, as described by *Shukla and Mo* [1983]. In this case, however, the ridge is located farther south than the normal winter blocking ridges, which are usually centered between 50°–70°N. This ridge is also not as strong as those described in the literature, at least in this composite, and does not persist in the ensemble averaged 5-day means beyond the period following the transition. Instead, the ridge disappears and is replaced by the pattern shown by the bottom panel of Figure 5, which persists (in the 5-day ensemble means) until at least the end of the 45-day period following the transition examined here. Thus the persistent pattern is that of diffluent contours of 500-mbar height, representing a weakening of the flow over North America. The combination of diffluent flow at 500 mbar with high pressure under the ridge and low pressure under the trough is a weak version of the vortex pair associated with atmospheric blocking [*Malanotte-Rizzoli and Malguzzi*, 1987; *Pierrehumbert*, 1986]. In the discussion section we argue that the persistence of the offshore high pressure is related to this diffluent upper level flow over North America.

4.2.2. *EOF and PEP analyses.* Figure 7 shows the first two EOFs of coastal ASL and coastal alongshore wind stress for the spring transition period. These two functions account for 93% and 94% of the variance in ASL and wind stress, respectively, over the 91-day periods around the spring transition. Comparing these to Figure 2 shows the similarity of the spatial patterns for both functions of both variables to the first two spatial functions for annual ASL. The first spatial function of ASL covering the spring transition shows a more uniform response in the middle and north of the domain than the annual function, decreasing only in the south at LA and MO. The first spatial function of alongshore wind stress has a maximum in the middle of the domain at CC and only decreases at the very southern end (LA). This highlights the large alongshore scale of the spring transition event. The maximum in the southward winds in the middle of the domain around 40°N is a well-known occurrence [*Nelson*, 1977; S1; S2]. The second spatial functions both show the same pattern of opposing motion in the north and south.

The time series for the first EOFs show that the wind stress associated with this mode is nearly zero before the transition, increases sharply to the south at the time of the transition (0.2–0.3 N/m^2), and remains strong after the transition (0.1–0.2 N/m^2). The time series for ASL demonstrates a nearly symmetric reversal around the time of the transition. Rather than covering a period of 2–3 months, as implied by Figure 2, most of the transition is seen to occur in a 5- to 10-day period. As with the time series for the annual case (Figure 2), the time series of the second spring transition EOFs for both variables

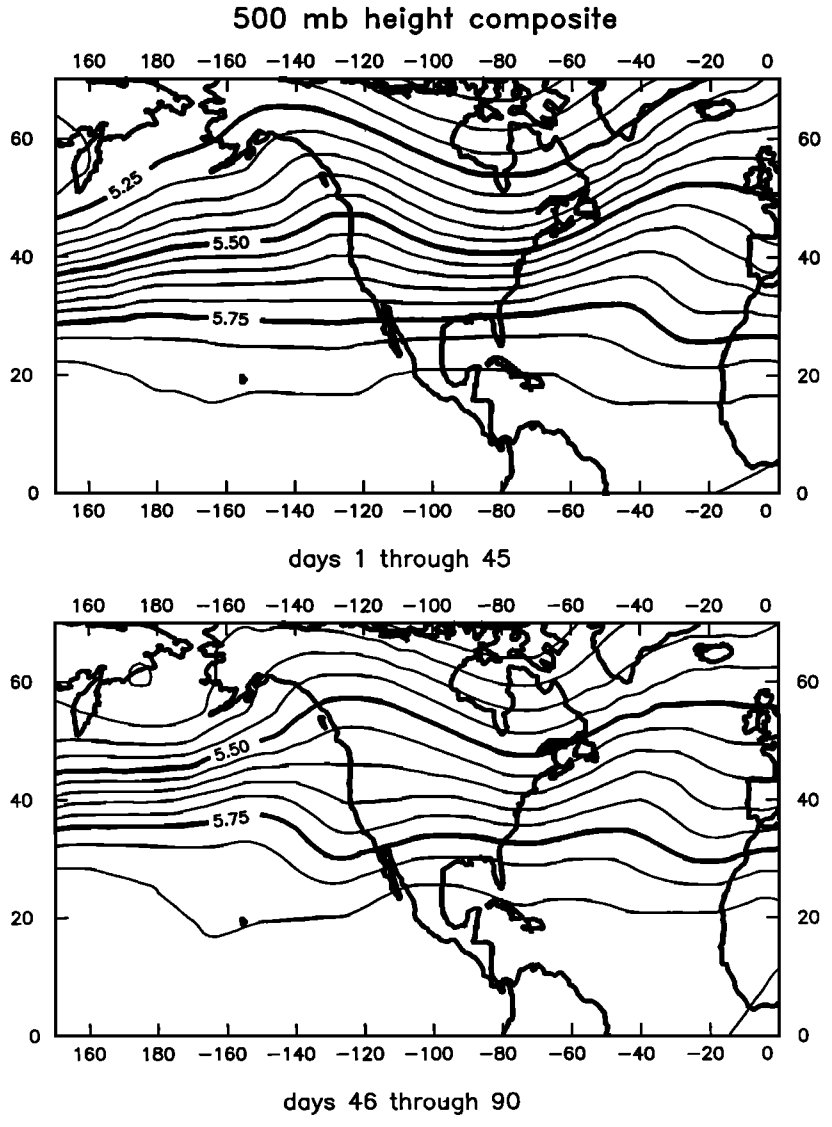

Fig. 5. Forty-five day mean 500-mbar fields composited from the 9 years before (top) and after (bottom) the spring transition. Contours are in kilometers, i.e., the contour interval is 50 m.

are strongest prior to the spring transition, corresponding to southward stress and low sea levels off southern California and northward stress and high sea levels off Oregon and Washington. This pattern is especially strong in the 10 days before the transition, representing the passage of storms through the northern region while southward winds increase off central and southern California, as seen in the composites of SLP.

The time series of the first modes of coastal ASL and alongshore wind stress are correlated at the 95% level over the 91-day records of all 9 individual years; the second modes are correlated at the 95% level for 7 of the 9 years. This is evident in the similarity between the composite time series for each of the modes, although there is more short-period variability in the wind stress. This statistical connection between alongshore wind stress and sea level response off northern California, Oregon, and Washington supports the conclusion from previous studies that the oceanic spring transition is forced by the large-scale winds. The weaker response seen in the low values of the first ASL EOF spatial functions off central and southern California is also consistent with previous observations of weak or nonexistent spring transitions there.

Figure 8 shows the spatial patterns and composite time series for EOFs 1, 2, 3, and 6 for SLP over the Pacific, accounting for 27, 22, 10, and 6% of the variance in the fields, respectively. Selection of these modes (out of the first 10 modes computed) is based on the correlation of their time series with the time series for the coastal ASL and alongshore wind stress modes. The highest correlation between Pacific SLP and coastal wind stress was for SLP mode 6, which correlates with the time series of the first alongshore coastal wind stress EOF at the 95% level for each of the 9 individual years. SLP modes 3 and 2 are correlated at the 95% level with the first wind stress mode for 7 and 6 of the 9 years, respectively. The other SLP modes (including the first) were not well correlated with the coastal alongshore wind modes during a majority of the years. In a similar manner the SLP modes 1 and 3 were most often correlated with the coastal ASL mode (during 7 and 6 of the 9 years, respectively).

The connection between the SLP modes 3 and 6 and the

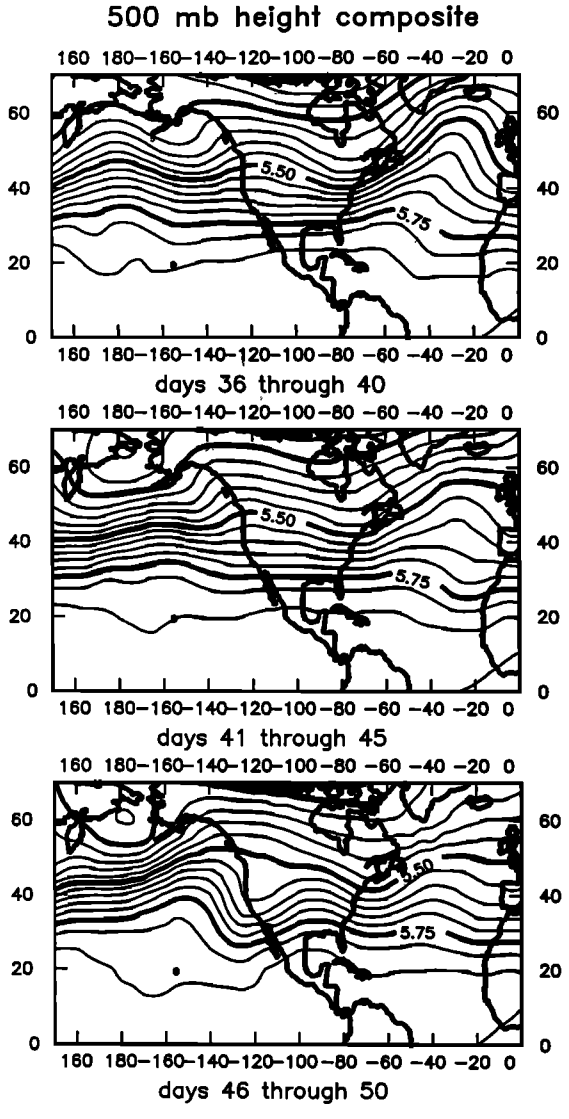

Fig. 6. Five-day mean 500-mbar fields composited from the 9 years: the two 5-day periods preceding the spring transition (top and center) and the 5-day period immediately after the transition (bottom).

coastal winds arises through the stronger cross-shelf gradients in pressure near the coast seen in the spatial patterns of those modes. As can be seen from the time series of the modes, the third and sixth modes reach their largest magnitudes at the time of the transition and maintain high mean magnitudes after the transition. The spatial patterns are concentrated in the northeast Pacific, in agreement with the composites of surface pressure fields shown in Figure 4. In addition, model 6 includes a low-pressure center over North America, as observed in Figure 4. Thus these two modes, accounting for 15% of the SLP variance, have both spatial and temporal characteristics similar to the observed pressure systems at the time of the transition and to the alongshore winds during the transition. Modes 1 and 2 of the SLP, on the other hand, account for a combined 49% of the variance in SLP over the large domain and appear to represent the larger-scale basin modes, with more slowly varying time series than modes 3 and 6.

The most straightforward method of showing the connection between the fields is the use of principal estimator patterns. Figure 9 shows the results of applying the PEP technique to SLP and ASL and to SLP and alongshore wind stress during the 91-day spring transition period. Results are shown for the first two PEPs, relating the first 10 SLP EOFs to the first six ASL or wind stress EOFs. Essentially all of the variance of the fields are contained in these EOFs. For both ASL and wind stress, the first PEP mode shows the main transition (time series becomes strongly positive during days -2 to $+1$), and the second PEP shows the conditions prior to the transition (time series strongly positive during days -12 to -2). For ASL and alongshore wind stress these two PEP modes are very similar to the first two raw EOF modes, and their interpretation is as described above. The new information provided by the PEP analysis is contained in the associated SLP patterns. Mode 2 shows the strengthening of the high pressure off California during the 10–15 days prior to the transition; at the same time the Aleutian low increases in strength, consistent with the passage of one or more storms through the Gulf of Alaska, British Columbia, and southward into the central United States. Mode 1 describes the rapid intensification of the high-pressure system in the NE Pacific at the time of the transition and the strengthened presence of the low pressure over the continental United States. When using the PEP method in a predictive manner, the amount of variance of the estimand explained by the estimator is called the hindcast skill. In that sense the 10 SLP EOFs explain 65% of the variance in the six alongshore wind stress modes and 51% of the variance in the six ASL modes. Most of the hindcast skill for ASL (92%) is contained in the first PEP mode, with most of the rest of the skill (7.3%) contained in the second. Thus these two patterns represent 98% of the connection between the large-scale atmospheric pressure and the coastal ocean, explaining approximately 63% of the variance in alongshore wind stress, 50% of the variance in the ASL, and 25% of the SLP variance during the 3-month spring transition period.

4.3. *Fall Transition*

4.3.1. *Composite events in the atmosphere.* Figure 10 is the counterpart of Figure 4. Figure 10*a* shows 30-day averages of the SLP, composited around the time of the fall transition, as determined from the rise in ASL at SB (Figure 1). These can be thought of as monthly means covering roughly September, October, and November. They show the deepening of the Aleutian low with the appearance of the 1008- and 1004-mbar isobars during the transition month and the near disappearance of the subtropical high. Note that the continental low over the United States is already absent in the top panel. Figure 10*b* shows averages over the two 15-day periods preceding and one 15-day period following the transition. The deepening of the Aleutian low appears to be a continuous process, while the subtropical high stays relatively constant in the top two panels. In the bottom panel the Aleutian low expands southward to 40°N along the coast after the transition and the subtropical high is moved to the central Pacific and greatly diminished. The movement of the 1020-mbar isobar offshore is shown in the 5-day averages of Figure 10*c*, covering the period from 10 days before to 5 days after the transition. Although the fall transition is less striking than the

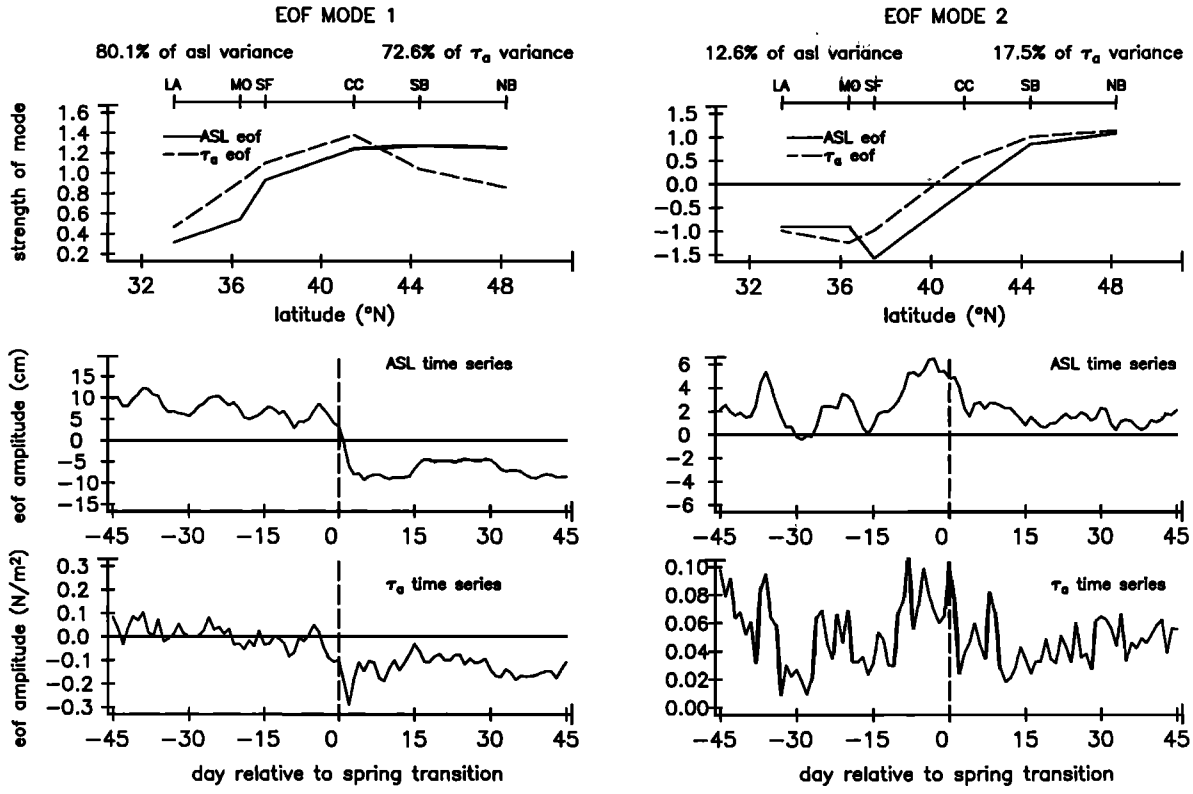

Fig. 7. The first two EOFs for the sea level and alongshore wind stress for the period surrounding the spring transition. Data are from the same locations as in Figure 2. These were calculated from nine appended 91-day records. The spatial functions for ASL (solid curves) and wind stress (dashed curves) are shown in the top panels. The 9-year averages of the time series of the EOF amplitudes are shown in the middle panel (ASL) and bottom panel (wind stress). The date of the transition is day 0.

spring transition, the expansion of the low to approximately 40°N and the final movement of the high pressure away from the coast takes place relatively rapidly. Composites of single days (equivalent to Figures 4*d* and 4*e*) are not shown. The SLP on days 45, 47, and 49 all look essentially like the 5-day mean at the bottom of Figure 10*c*, and the winds are as expected for nearly geostrophic flow, northward along the coast, stronger north of 40°N than south.

Figures 11 and 12 present the patterns in 500-mbar heights and are the counterparts of Figures 5 and 6. Figure 11 shows the seasonal change with 45-day averages of the composite 500 mbar heights, before and after the transition. The mean picture after the fall transition (Figure 11, bottom) is similar to the mean picture before the spring transition (Figure 5, top), with zonal flow south of around 30°N and a ridge over western North America north of that. The situation before the fall transition (Figure 11, top) is not as strongly divergent over the coast as it was after the spring transition (Figure 5, bottom). This is mostly due to the lack of a strong trough over the coast south of 40°N before the fall transition. Figure 12 shows 5-day averages of the composite 500-mbar heights covering the period from 10 days before to 5 days after the transition. The pattern is not simply a reversal of the spring transition progression (Figure 6), although there are similarities. The top panel shows more divergence than seen in the 45-day average at the top of Figure 11. It is similar to the 5-day average following the spring transition, although the low pressure over the continent is less pronounced. The ridge and trough pattern seen in the middle panel is also less divergent than the picture following the spring transition. This pattern is rapidly replaced by the reverse, trough and ridge pattern at the time of the fall transition. Combined with the extension of the Aleutian low southward to 40°N, this describes a synoptic storm that continues to be visible through the next 5-day mean (not shown). The fall transition thus occurs at a time when storm conditions prevail over the northwest for a period of roughly 10 days. The 5-day means then begin to resemble the bottom panel of Figure 11, lacking the strong trough off the west coast. The net effect is to move the center of strong, westerly, upper level atmospheric flow to the south of its location prior to the transition.

4.3.2. *EOF and PEP analysis.* Figure 13 shows the EOF spatial patterns and time series for the first two EOFs of ASL and alongshore wind stress for the time series centered on the fall transition. These two modes account for 90% of the variance for both variables. Prior to the transition, the sea level is dominated by the second mode, since the time series of the first mode is near zero. Sea level is highest in the south at SF (both time series and spatial function are negative), decreasing between SF and SB. The winds at that time are a combination of both modes. The first mode (at this time) describes a mean southward stress (negative time series), greatest in the north at about 0.08 N/m^2, falling to less than half of that south of SF. The second mode describes winds that blow northward in the

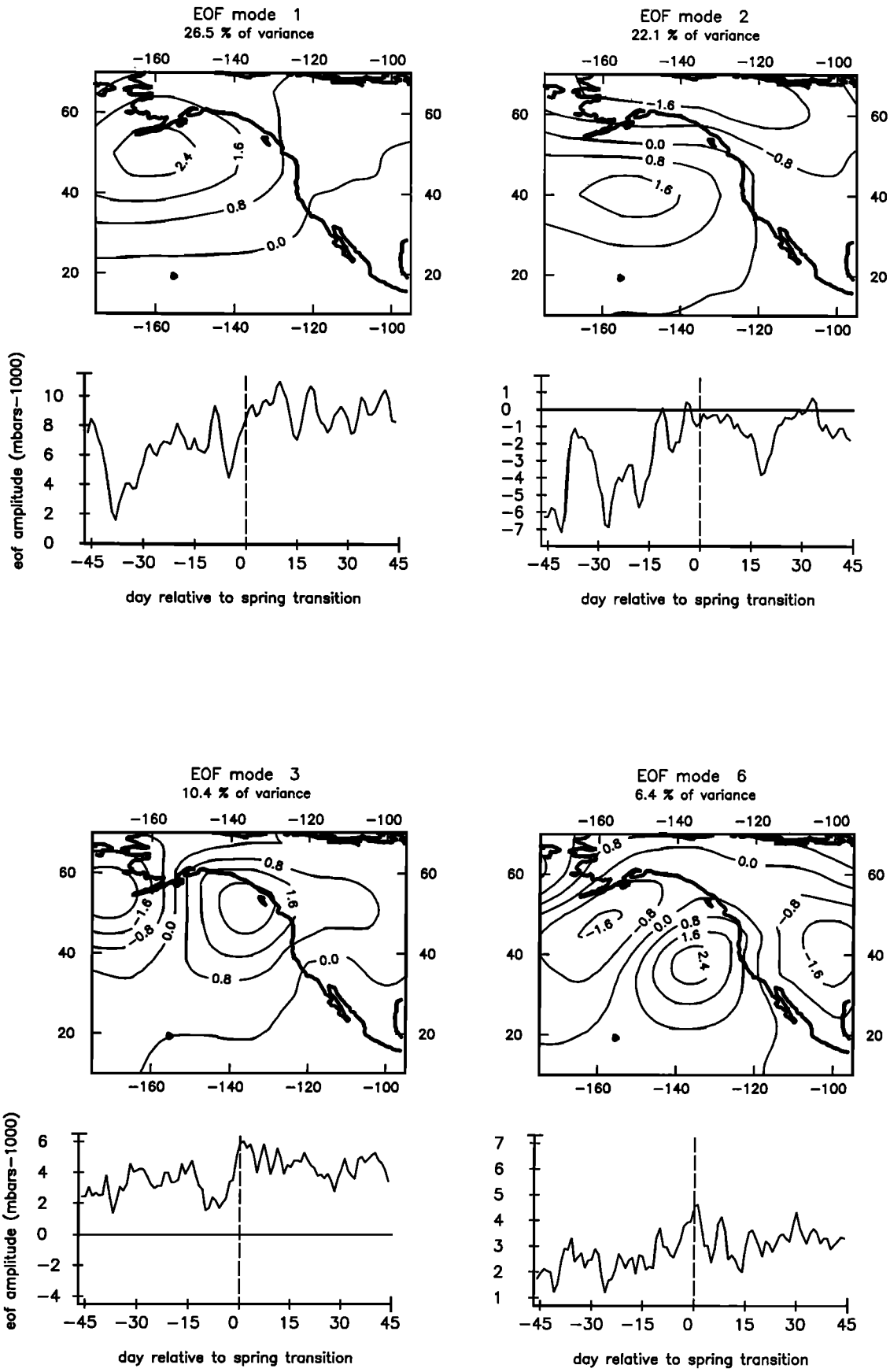

Fig. 8. The four EOFs of the SLP that are most correlated with ASL and alongshore wind stress for the period surrounding the spring transition. Spatial functions are shown at the top; the 9-year averages of the time series of the EOF amplitudes are at the bottom. (*a*) Modes 1 (left) and 2 (right). (*b*) Modes 3 (left) and 6 (right).

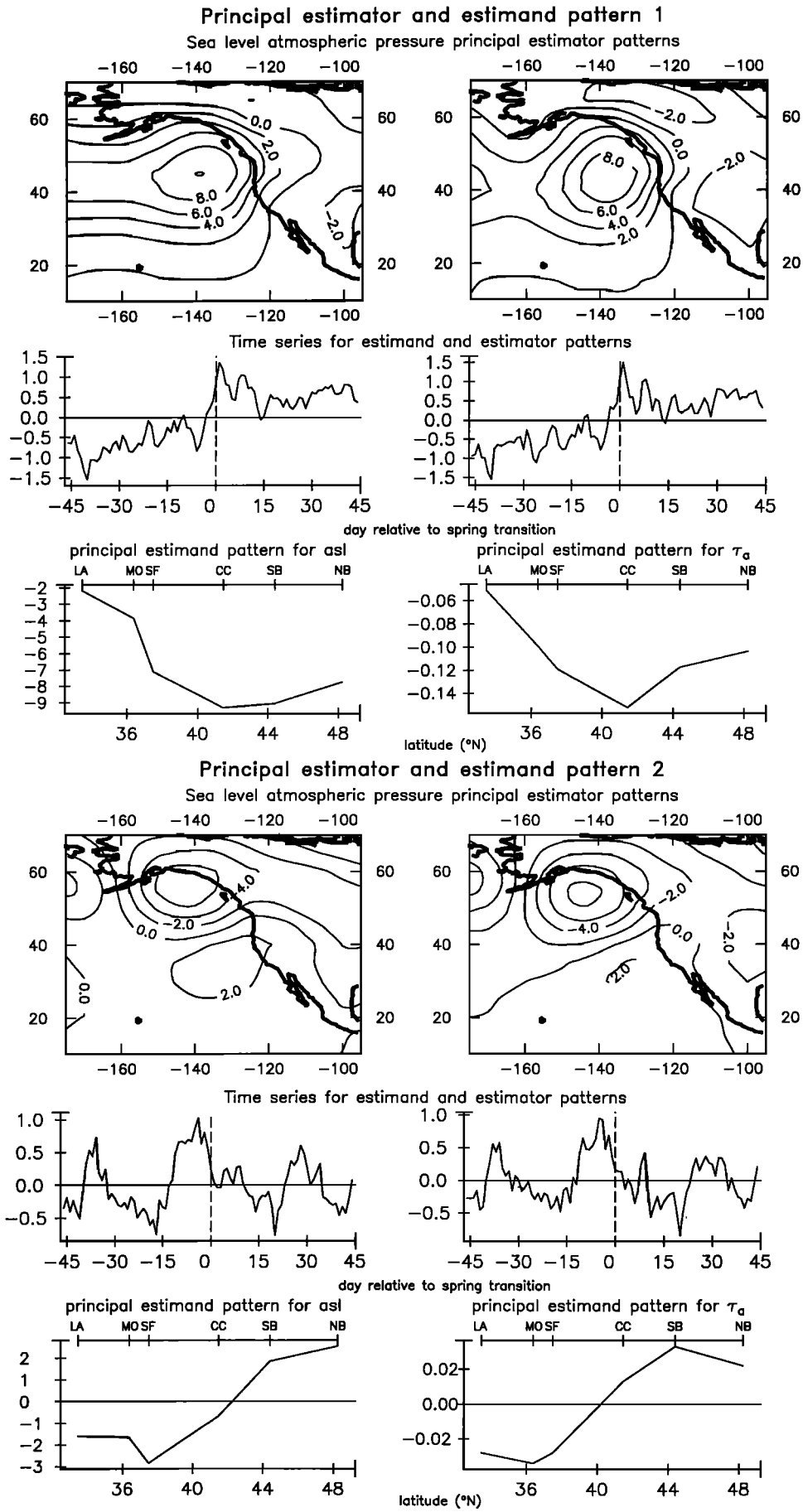

Fig. 9. Principal estimator patterns relating SLP to ASL (left) and alongshore wind stress (right) for the spring transition. The spatial patterns for SLP are shown at the top; the spatial pattern for the other variable is shown at the bottom; the common time series is shown in the middle. SLP is the estimator; the estimand is the other variable. (*a*) First PEP; (*b*) second PEP.

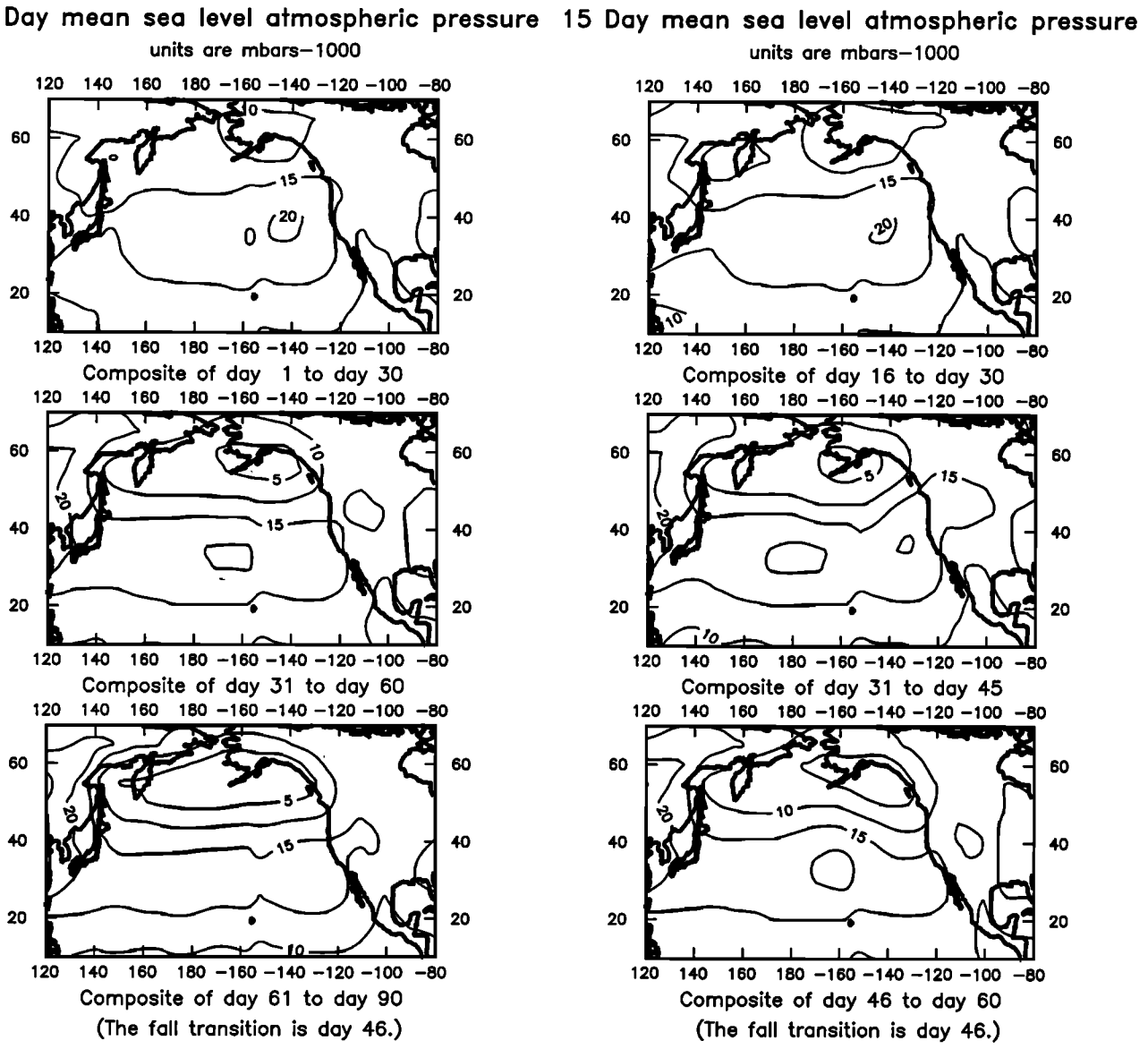

Fig. 10. Atmospheric SLP fields from before and after the fall transition. As in Figures 4*a*–4*c*, except for the 91-day period surrounding the fall transition. (*a*) Thirty-day means covering 90 days. The transition occurs during the middle of the period covered by the center panel. (*b*) Fifteen-day means of SLP. The transition occurs between the periods covered by the center and bottom panels. (*c*) Five-day means of SLP. The transition occurs between the periods covered by the center and bottom panels.

north and southward in the south, with pulses of about 0.05 N/m^2 in both directions. After the transition the time series of the wind stress first mode becomes positive, describing northward winds everywhere, and is greater in the north (approximately 0.1 N/m^2). The second mode of the wind stress continues to alternate, adding another 0.1 N/m^2 of northward wind in the north, corresponding to winds during storms that do not penetrate south of approximately 40°N. The compositing over the 9 years reduces the peak strength of these storm winds. Individual years show peaks of 0.4–0.6 N/m^2 in the north during these pulses and also show an increase in the strength of these pulses following the transition. After the transition the relative slope of the sea level is described by the first mode, a south to north upward slope between LA and SB. The response in the fall gives rise to a more linear slope in the first EOF than in the spring, when the drop in sea level is nearly uniform between SF and NB. In the fall the strong forcing and response are concentrated in the north, with a linear decrease south of SB. Thus a rapid transition is seen in the time series for sea level and wind stress (mode 1), but the magnitudes of the jumps are less than those seen in spring, and the forcing and response are confined more to the north.

EOFs of SLP during the fall transition were calculated but are not shown. In general, modes 1, 2, 3, and 6 are very similar in appearance to the modes found for the spring transition (Figure 8), with slight differences in the locations of the maxima between the corresponding modes of the two transitions. Correlations between these and the first two modes of ASL and coastal alongshore wind stress reveal that SLP mode 3 is most correlated with the first mode of the wind stress and ASL, and SLP mode 6 is most correlated with their second modes. As with the spring transition, modes 3 and 6 (es-

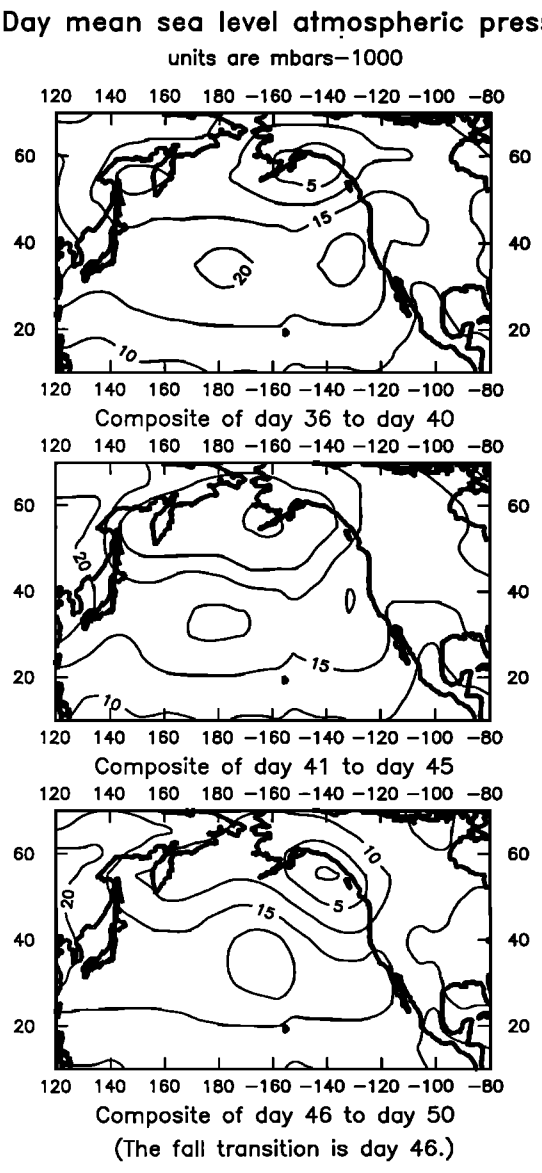

Fig. 10. (continued)

pecially 3) represent the northeast Pacific pattern, and modes 1 and 2 represent the large-scale North Pacific pattern. Modes 1 and 2 show more gradual changes in their time series, while mode 3 has the most dramatic change at the time of the transition. The fact that of the EOFs for two different periods of the year are very similar may indicate their robustness in describing the atmospheric systems that occur with varying strength at different times of the year; it may also indicate a domain shape dependence as described by *Richman* [1986].

The PEP analysis for the fall transition period is shown in Figure 14. The spatial and temporal patterns for ASL and alongshore wind stress PEP modes are similar to their first two raw EOF patterns (except for the reversal of sign of the first modes). A difference can be seen in the ASL modes, which are more like the wind stress in both PEP modes than they were in the raw EOF modes. The first raw EOF time series for ASL (Figure 13) was zero before the transition, relying on the second mode to maintain the relative alongshore slope. In the PEP analysis (Figure 14) this slope is maintained by the first mode before the transition, then reversed and maintained in the opposite direction after the transition, again by the first mode. The second ASL and wind stress PEP modes are similar to each other, describing opposing ASL and wind in the north and south. Our interpretation is that the second PEP pattern corresponds to strengthened storm conditions in the Gulf of Alaska at the same time that the North Pacific high remains strong south of ~50°N. There is a period of strengthening in this mode around 10 days before the transition, corresponding to a slight increase in the relative slope in ASL prior to the fall transition. Several days before the transition the strength of the first mode increases (large negative time series), and the Aleutian low expands to drive northward winds along most of the coast, with greater strength north of 40°N.

The hindcast skill during fall is less than during spring. The 10 SLP EOFs explain 56% of the variance of the alongshore wind stress and 34% of the variance of ASL. The first PEP pattern is not quite as dominant, accounting for 81% of hindcast skill for ASL and 89% for wind stress. Overall, the first two PEP modes still account for 97–98% of the connection between SLP and both ASL and alongshore wind stress. The modes associated with SLP and ASL account for 21% of the SLP variance over the 3-month fall transition period.

5. Discussion

As stated in the introduction, the primary goal of this paper is to characterize the atmospheric events which force the spring and fall oceanic transitions. A secondary benefit of the EOF analysis sea level is a more concise picture of the nature of the oceanic transitions themselves. The previous section presents and this section discusses in more detail the ensemble averaged atmospheric fields and modes. These show the nature of the events in a mean sense but eliminate interannual variability. A complete examination of the details of the interannual variability is beyond the scope of this paper, but we will briefly discuss the transitions from individual years to assess the degree to which the composites represent what happens on any given year.

5.1. *The Ensemble Mean Transitions*

5.1.1. *Coastal ASL and wind stress.* Figures 2, 7, and 13 present a consistent picture of the behavior of the coastal alongshore wind stress and sea level during the transitions. During spring, approximately 80% of the variance in ASL and 70% of the variance in alongshore coastal wind stress are explained by their respective first EOFs, depicting a large-scale drop in sea level during a southward wind event. During fall, approximately 65% and 75% of the variance in ASL and wind stress, respectively, are explained. The forcing and response are opposite to those in spring (northward winds drive sea levels high) and are more confined to the region north of 40°N. The first modes show sharp transitions during both spring and fall, with wind stress leading sea level; the transition is more pronounced in spring than in fall. The second modes have opposite signs in the north and south and explain all but approximately 10% of the remaining variance. The second mode of ASL is important before each of the transitions. Before the spring transition it describes a drop in sea level in the south while sea level remains high in the north. Before the fall transition it dominates the picture, depicting high sea levels in the south and low levels in the north. The

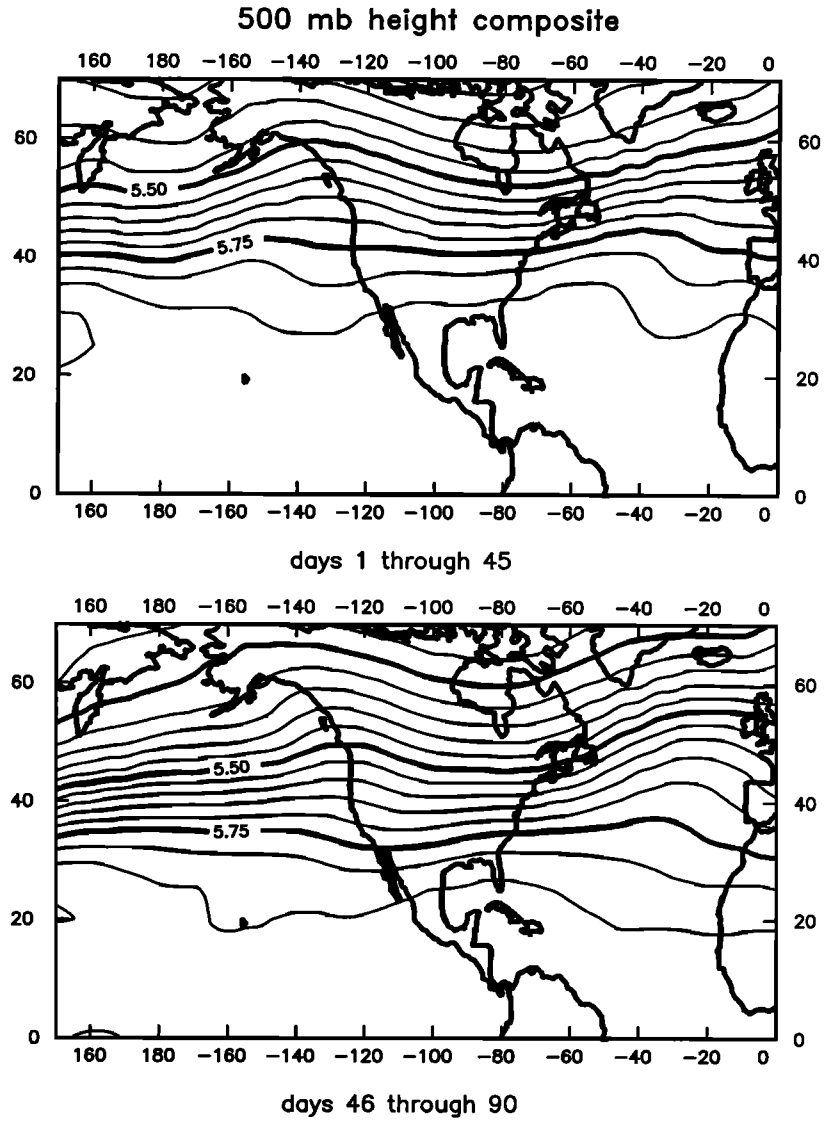

Fig. 11. Forty-five day mean 500-mbar fields composited from the 9 years, as in Figure 5 except for the fall transition: before (top) and after (bottom) the fall transition.

second mode of wind stress describes northward winds in the north and southward winds in the south, usually attributed to storms passing north of the subtropical high-pressure system. It decreases during the spring transition and increases after the fall transition, although it is already active before the fall transition.

Another view of the oceanic transition is obtained by using the first two EOFs of ASL (accounting for over 90% of the variance) to reconstruct the sea level time series at each station. Alongshore profiles of ASL for days preceding and following the spring and fall transitions are shown in Figure 15. These represent the evolution of the relative (not absolute) alongshore slopes. If there is a long-term mean alongshore slope, this should be added to the slopes in Figure 15 to show the evolution of the absolute alongshore slope. Figure 15 shows the increase in the relative north-south slope approximately 5 days before the spring transition. Two days after the transition, this slope is nearly flat between SF and NB. In the south (LA to SF) the relative slope is upward-to-the-south, opposing the upwelling regime. Addition of the mean annual *Hickey and Pola* [1983] slope (not shown) increases the upward-to-the-south slope in the south and leaves a slightly larger upward-to-the-north slope in the north after the transition (a rise of 4–6 cm between CC and NB). In the fall the relative slope prior to the transition is weak, with a slight steepening of the upward-to-the south slope between 5 and 2 days before the transition. This slope reverses by 2 days after the transition and continues to increase (upward-to-the-north) after that. Adding the Hickey and Pola mean slope in the fall flattens the slope in the south (LA to SF) after the transition and increases it slightly in the north. The important point of this reconstruction, however, is to show the rapid changes in the alongshore slope in spring and fall, rather than the slow changes implied by monthly means, such as those given in *Hickey and Pola* [1983].

5.1.2. *The connection to SLP and the middle atmosphere.* The connection between SLP and the coastal ASL is best brought out by the PEP analysis (Figures 9 and 14). The

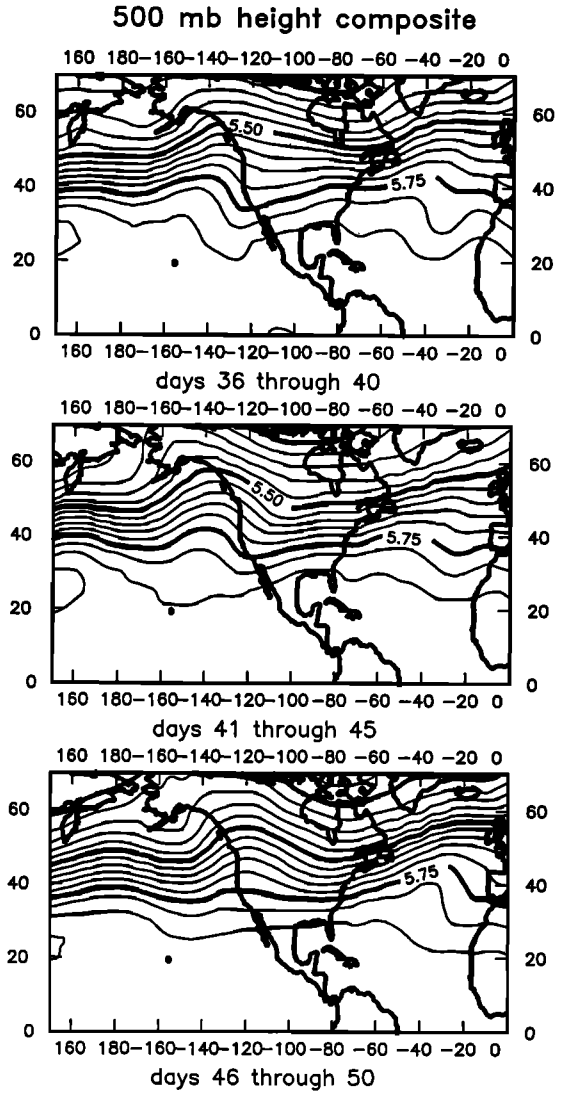

Fig. 12. Five-day mean 500-mbar fields composited from the 9 years, as in Figure 6 except for the fall transition: the two 5-day periods preceding the fall transition (top and center) and the 5-day period immediately after the transition (bottom).

first and second SLP modes for spring are similar to those for fall. The first shows the rapid increase (spring) or decrease (fall) in pressure over a region covering the northeast Pacific Ocean centered at approximately 140°W and 45°N. It also shows a coincident decrease or increase in pressure over the United States. The second SLP mode depicts low pressure in the north and high pressure in the south, interpreted as storms passing north of the subtropical high. The time series for this mode fluctuates but has a maximum before the spring transition and possibly before the fall transition.

Combination of the SLP and 500-mbar height fields provides the best picture of the nature of the spring and fall transition atmospheric events. In Figure 16 the 9-year mean fields of these two data sets are presented for the day following the spring and fall transitions. Conditions during the fall transition (bottom panel) are characteristic of midlatitude synoptic storms (500-mbar trough over a surface low), although the ensemble averaging weakens the features in comparison to the instantaneous features of any one storm and makes it difficult to tell whether the 500-mbar trough is west of the surface low. These conditions appear to persist over a period of 5–10 days, corresponding to a sequence of several storms. Before this event the 500-mbar heights show a region of zonal flow north of 40°N (Figure 11). During the transition this region moves south and then remains in place, bringing the storm track to its normal winter position over the west coast. In this sense it appears to represent a rapid event (change in position of the storm track).

During the spring transition (Figure 16, top) the 500-mbar ridge situated over the high surface pressure in the northeast Pacific is similar in some respects to atmospheric blocking [*Rex*, 1950*a*, *b*; *Charney et al.*, 1981; *Shukla and Mo*, 1983; *Dole*, 1986]. Several studies have found a maximum in the number of blocking events in spring [*Rex*, 1950*b*], although *White and Clark* [1975] found a maximum over the North Pacific in fall and winter and a minimum in spring and summer. The large-scale pattern associated with atmospheric blocking consists of a region of diffluent 500-mbar flow (a ridge north of a trough) downstream of a strong zonal flow; high and low surface pressure cells are found under the ridge and trough, respectively. There is a baroclinic slant to the pressure systems during the set up phase but the final, quasi-stationary system is nearly barotropic. The north-south dipole structure under the diffluent flow is very stable and can be described as a modon [*McWilliams*, 1980] or as a local quasi-stationary Rossby wave [*Malanotte-Rizzoli and Malguzzi*, 1987]. A number of studies have shown that eddies formed in the upstream region of strong zonal flow contribute to the stability of the diffluent, dipole structure through an eddy vorticity flux [*Schutts*, 1983, 1986; *Pierrehumbert*, 1986; *Malanotte-Rizzoli and Malguzzi*, 1987; *Haines and Marshall*, 1987]. Malanotte-Rizzoli and Malguzzi find that the presence of the diffluent jet creates a potential vorticity field that acts as a potential well, trapping the incoming eddies to reinforce the dipole structure.

Is the expansion of the high-pressure system during the spring transition a blocking event? Figure 17 shows 5-day means of 500-mbar heights and SLP for the 15 days before and after the transition. The high-pressure system in the northeast Pacific is the southern member of a pressure dipole (low-north-of-high) at the downstream end of a region of confluent flow, rather than the opposite. During the 5 days following the transition the high pressure does lie under a 500-mbar ridge. After that, however, a weak version of the diffluent flow pattern normally associated with blocking occurs over the continent, with a dipole of SLP (high-north-of-low) under the diffluent flow. One of the characteristics of the blocking dipole is a meridional elongation of the pressure systems, which can be seen in the region of low pressure over the southwest United States.

Thus the high pressure in the NE Pacific is only associated with a 500-mbar ridge for approximately 5 days following the transition. After that a weakened version of the typical blocking pattern develops over North America at the time of the transition and is relatively stable afterward. The high-pressure system in the northeast Pacific is part of a dipole pressure system (low-north-of-high) upstream from the diffluent flow and pressure dipole typical of blocking (high-north-of-low). The double dipole is strongly evident on the day following the transition (Figure 16, top). *Pierrehumbert* [1986] shows this

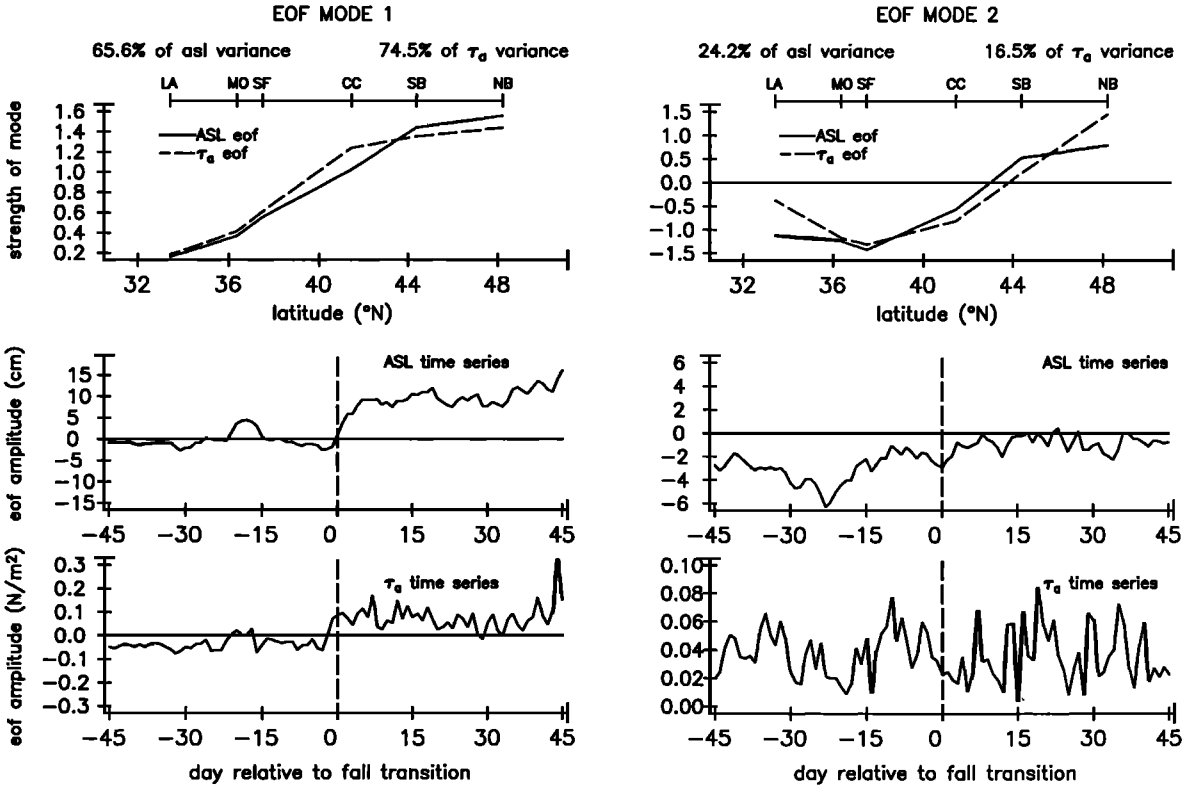

Fig. 13. The first two EOFs for the sea level and alongshore wind stress for the period surrounding the fall transition. As in Figure 7 except for the fall transition.

type of double dipole to be one possible response of a barotropic fluid to the eddy vorticity flux associated with eddies moving from the strong zonal flow into the diffluent region. *Haines and Marshall* [1987] use a nonlinear equivalent barotropic model to illustrate the way in which the eddies moving into the diffluent region maintain the dipole. It is interesting to note that Figure 9 of Haines and Marshall, depicting the evolving eddy field, shows a high pressure cell located upstream of the dipole much of the time. We suggest that the persistence of the North Pacific high following the spring transition is due to its participation in the very persistent larger-scale structure consisting of the double dipole of SLP under a 500-mbar flow with upstream confluence and downstream diffluence. The upstream dipole may help to maintain the dipole under the diffluent flow through eddy fluxes of vorticity. A full analysis of potential vorticity fields in the atmosphere at the time of transition, such as conducted for winter blocking by *Schutts* [1986] and *Malanotte-Rizzoli and Hancock* [1987], might further clarify the dynamics of the atmospheric transition.

5.2. *Validity of the Composites = Interannual Variability*

The use of ensemble-averaged composite events brings out the underlying simple structure of similar events. It has the weakness, however, of masking a great deal of variability in the individual events and in the worst case may create the appearance of structure where none exists. This could be especially true in the present case. One can imagine a signal composed of a synoptic (3–10 day) periodicity superimposed on a seasonal cycle. Choosing a synoptic event at the time of the maximum rise in the seasonal cycle on each year and compositing the data around the start of the synoptic event could result in a composite showing a sharp transition. In this section we present data from individual years in an effort to assess whether the transitional nature of the composite is evident in individual years.

Interannual variability in the sea level signal can be seen in Figures 1 and 3. Considering the 91-day periods surrounding the transitions, Figure 1 shows that the oceanic transitions are often quite sharp, persisting for at least 15 days and usually longer. It is usually (but not always) easy to distinguish the transition event from previous events in spring but is more difficult in fall. In general, the composite (9-year mean) time series for the first EOF of ASL (Figures 7 and 13) is a valid representation of the nature of the transition events on individual years, especially in spring.

Interannual variability in the large-scale SLP and the representativeness of the 9-year composite can be seen in the time series of the first SLP-ASL PEP mode for the individual years (Figure 18). There appears to be more variability in the atmosphere prior to the transition than in the sea level (Figure 1), but a close comparison of Figures 18 and 1 shows a fairly good correspondence between atmospheric and oceanic

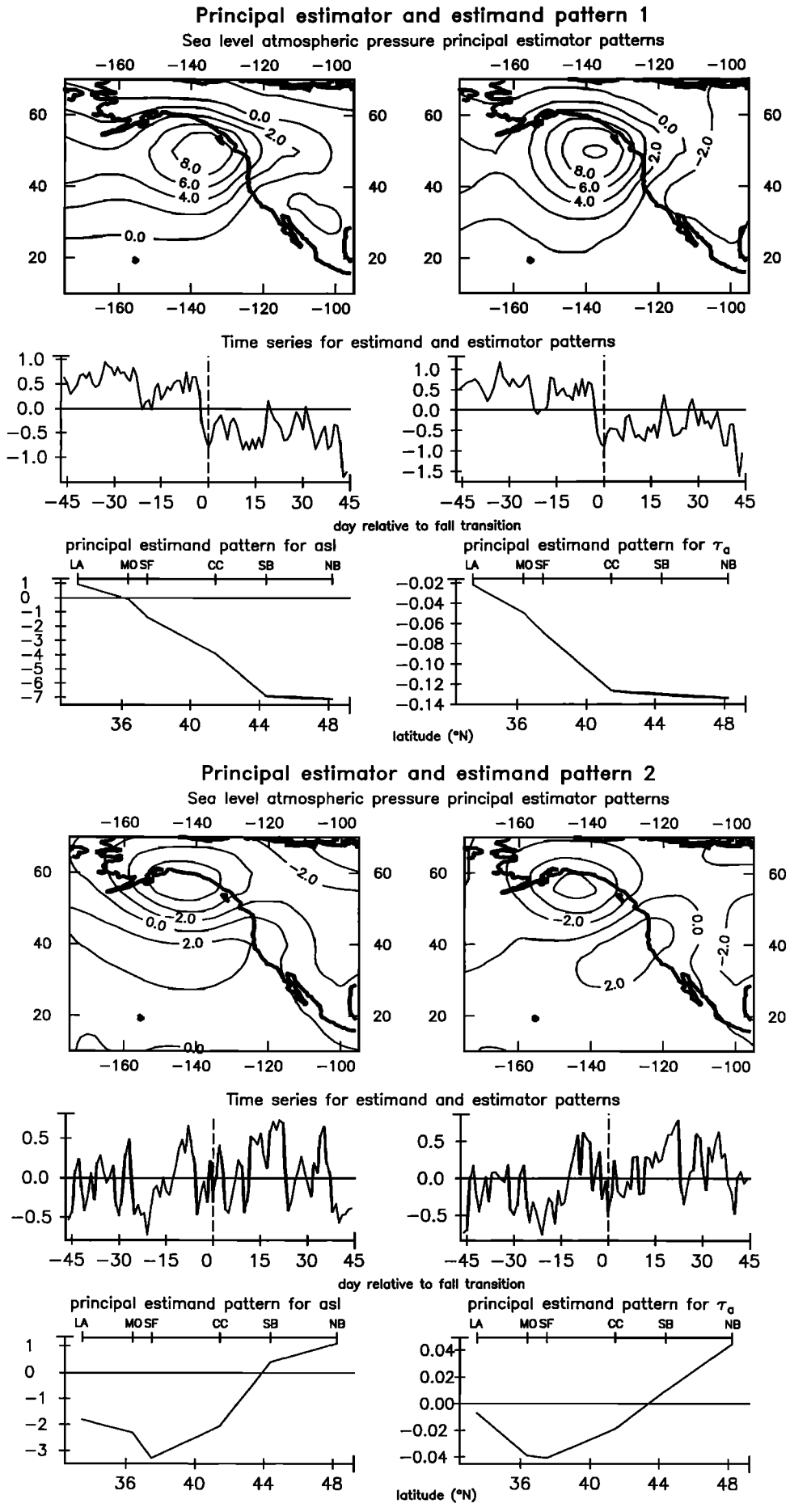

Fig. 14. Principal estimator patterns relating SLP to ASL (left) and alongshore wind stress (right) for the fall transition. As in Figure 9 except for the fall transition. (*a*) First PEP; (*b*) second PEP.

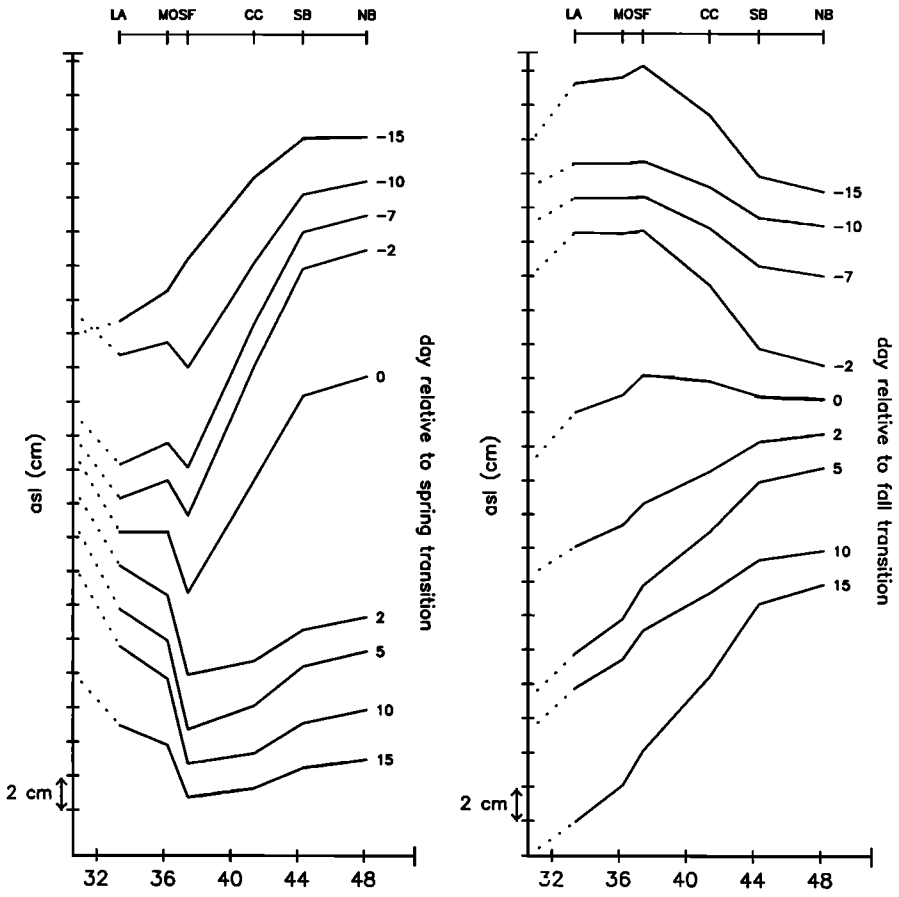

Fig. 15. Reconstruction of the relative slopes of alongshore sea level for days before and after the spring (left) and fall (right) transitions. No attempt to adjust these to include a mean annual alongshore slope has been made. The scale is the same for both plots, 2 cm per tic mark. The dotted curve on the left references each alongshore profile to a common height. Day numbers are shown to the right of each profile; the transition day is day 0.

events. The oceanic response appears more persistent than the atmospheric signal, as noted originally for the spring transition by *Huyer et al.* [1979]. For the spring transition the years in Figure 1*a* with reversals in sea level after the transition have similar reversals in the atmospheric pressure signal (1980, 1983). Thus the spatial and temporal patterns shown by the first PEP mode for SLP-ASL represent the nature of the atmospheric event which forces the oceanic spring transition. This does not occur on all years (for instance, 1971), but it occurs often enough to support the existence of a rapid transition in the pattern of SLP in the NE Pacific in spring. In the fall, however, the transitional nature of the atmospheric SLP is less evident. The SLP signal in Figure 18*b* is qualitatively like a synoptic signal superimposed on a slowly varying seasonal cycle, whereas the ASL signal in fall (Figure 1*b*) does display a transitional appearance.

6. Conclusions

6.1. *Spring Transition*

There is a rapid expansion of the high-pressure system in the NE Pacific at the time of the spring transition, concentrated in the region 20°–50°N and 120°–160°W (Figures 4 and 9). A more gradual increase in pressure over the larger-scale North Pacific also occurs over a period of 1–2 months, as seen in the first two EOFs of SLP (Figure 8). In the 5 days prior to the transition the Aleutian low strengthens at the same time that the high pressure builds off California, resulting in an increase in the upward-to-the-north slope of coastal sea level just before the transition (Figure 15). The expansion of the high pressure in the 5 days following the transition coincides with a ridging of the 500-mbar height field over the high pressure (Figures 16 and 17). This ridge does not persist beyond the 5–10 days following the transition; rather, the 500-mbar flow evolves into a stronger diffluent pattern over the continent of North America than existed prior to the transition, downstream of strong zonal flow over the NE Pacific (Figures 5 and 17). The SLP pattern after the transition resembles a double dipole, with low SLP north of high SLP in the NE Pacific and high SLP north of low SLP over the continent (Figures 16 and 17). This pattern persists in the ensemble 9-year mean over the next month and a half. We suggest that the relative persistence of the high SLP in the NE Pacific is due to the stability of the larger-scale pattern consisting of the double dipole of SLP and the diffluent jet at 500 mbar. Examination of first PEP time series from individual years (Figure 18) suggests that in many years there is a truly transitional nature in the SLP, although there is greater variability in the atmosphere than in the sea level, and on some years this transition is not seen.

The oceanic transition in sea level occurs over a period of several days, as described previously. Sea levels drop in the

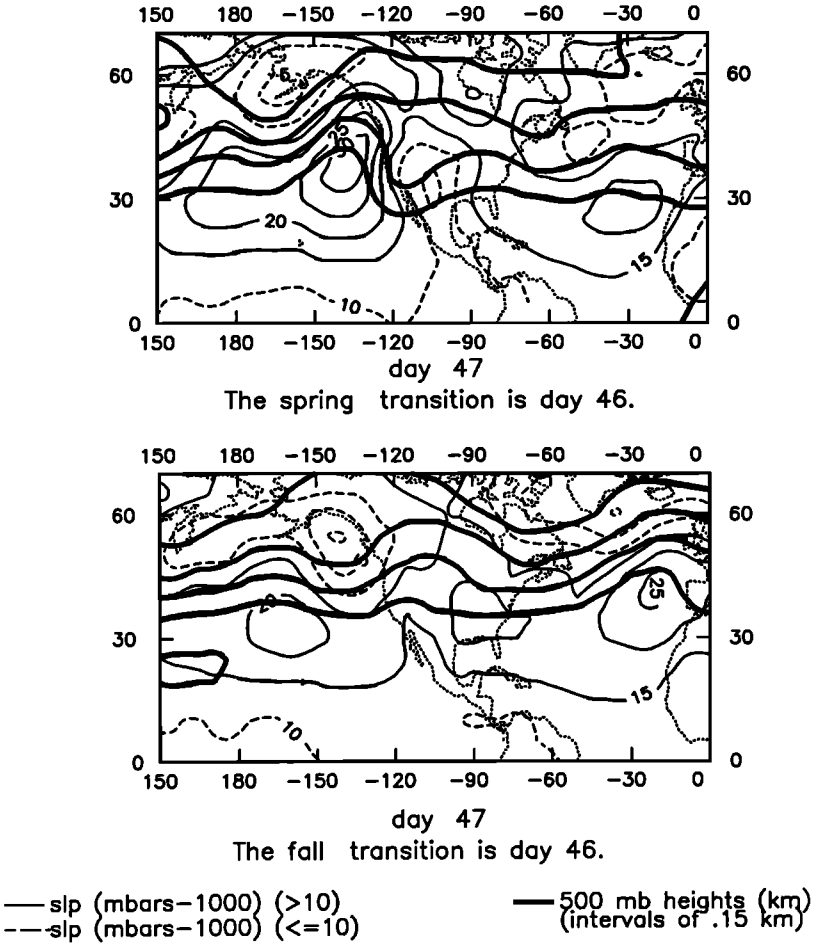

Fig. 16. Daily 9-year composite fields of 500-mbar heights (dark contours) and SLP (light contours, dashed for SLP ≤ 1010 mbar) on day 47 (one day after the transition) for the spring (top) and fall (bottom). Contour intervals are 0.15 km for 500-mbar heights and 5 mbar for SLP.

south and rise in the north during the steepening that precedes the transition, then sea level drops rapidly everywhere during the 2 days following the transition. The response is such that the relative alongshore slope between SF and NB (37°–48°N) is nearly gone 2 days after the transition (Figure 15). A small upwelling-favorable slope remains in that region (2 cm over 1200 km) after the transition, and this may be underestimated slightly due to the omission of the long-term mean slope. A stronger downwelling-favorable slope develops in the south between LA and SF (4 cm over 450 km), which may again be an underestimate. This downwelling-favorable slope may explain the weaker response in alongshore currents in the south seen by S1.

6.2. *Fall Transition*

The atmospheric pattern associated with the oceanic fall transition is that of a synoptic storm. The Aleutian low deepens and expands southward (Figures 10 and 14) under a 500-mbar trough (Figures 11, 12, and 16). In the 9-year ensemble mean this has the appearance of a monotonic transition, shifting the 500-mbar jet southward. Examination of the first PEP time series from individual years, however, reveals greater variability than during the spring transition (Figure 18). Although some years have a transitional appearance, the general pattern is that of synoptic scale variability superimposed on a gradual seasonal progression.

In the oceanic regime there are both gradual and abrupt aspects. By the time of the fall transition in late October through early November, sea levels have risen to a point half way between their May low and winter high (first EOF time series in Figure 2). An upward-to-the-south alongshore relative slope in sea level is concentrated between SF and SB before the transition (Figure 15). During the transition storm the response in sea level is concentrated toward the north around SB and NB, 45°–48°N (Figure 15). The 9-year composite time series of ASL and alongshore wind stress do appear transitional; the sea level records from individual years at SB (Figure 1) also show a monotonic rise on many of the years, in contrast to the first PEP time series (Figure 18). The upward-to-the-north relative slope continues to increase in the 15 days after the transition, which is a more gradual behavior than is seen in spring (Figure 15). Thus the final rise in sea level does have a transitional nature in the oceanic ASL regime, although it is weaker than in spring and concentrated more in the north. The change in atmospheric SLP, however, does not appear as a monotonic transition in fall.

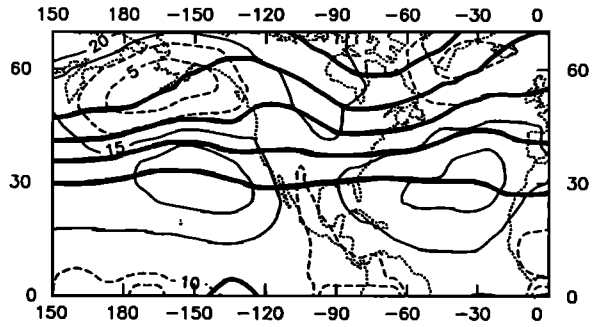

composite of days 31 through 35

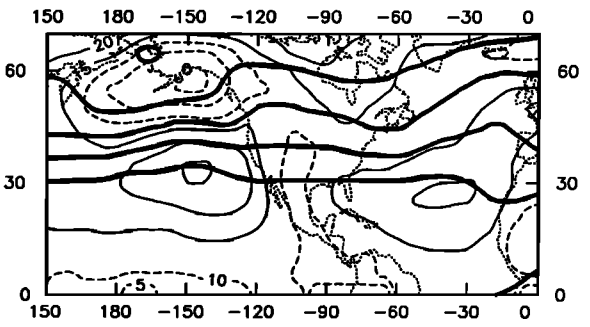

composite of days 41 through 45

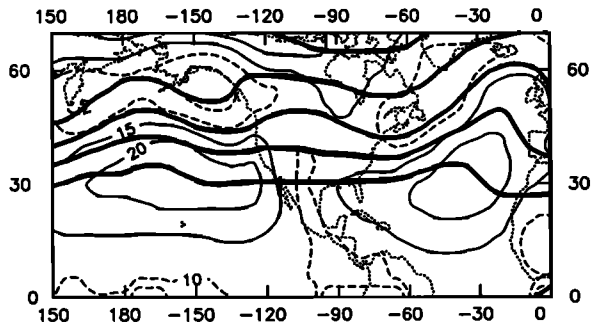

composite of days 36 through 40

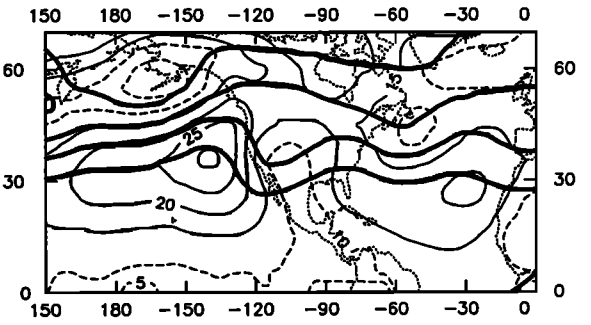

composite of days 46 through 50

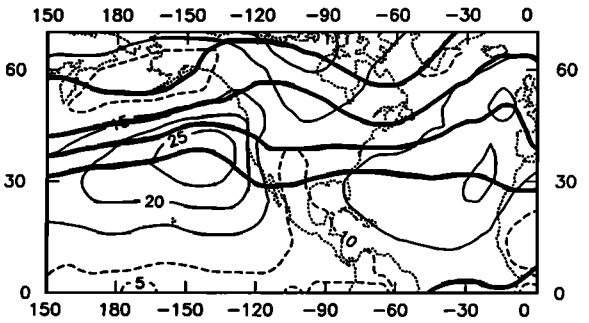

composite of days 51 through 55

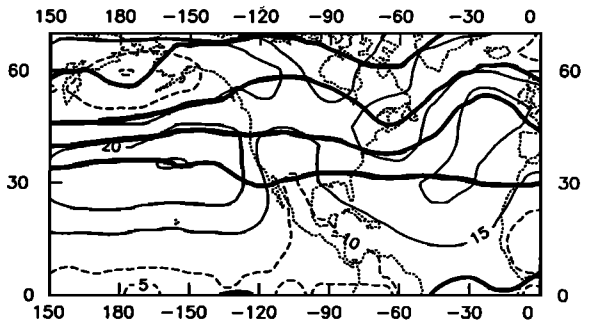

composite of days 56 through 60

Fig. 17. Five-day averages of 9-year composite fields of 500-mbar heights and SLP, as in Figure 16 except for the three five-day averages preceding and following the transition. The transition is day 46. (*a*) Days 31–35 (top) and days 36–40 (bottom); (*b*) days 41–45 (top) and days 46–50 (bottom); (*c*) days 51–55 (top) and days 56–60 (bottom).

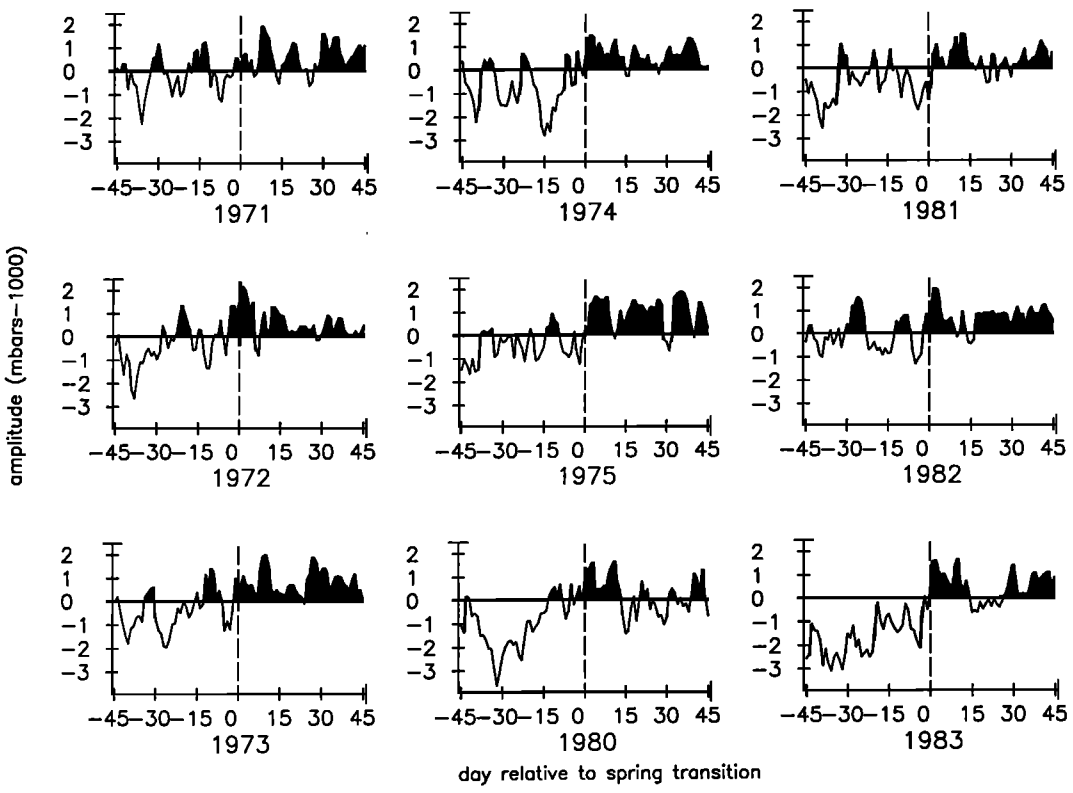

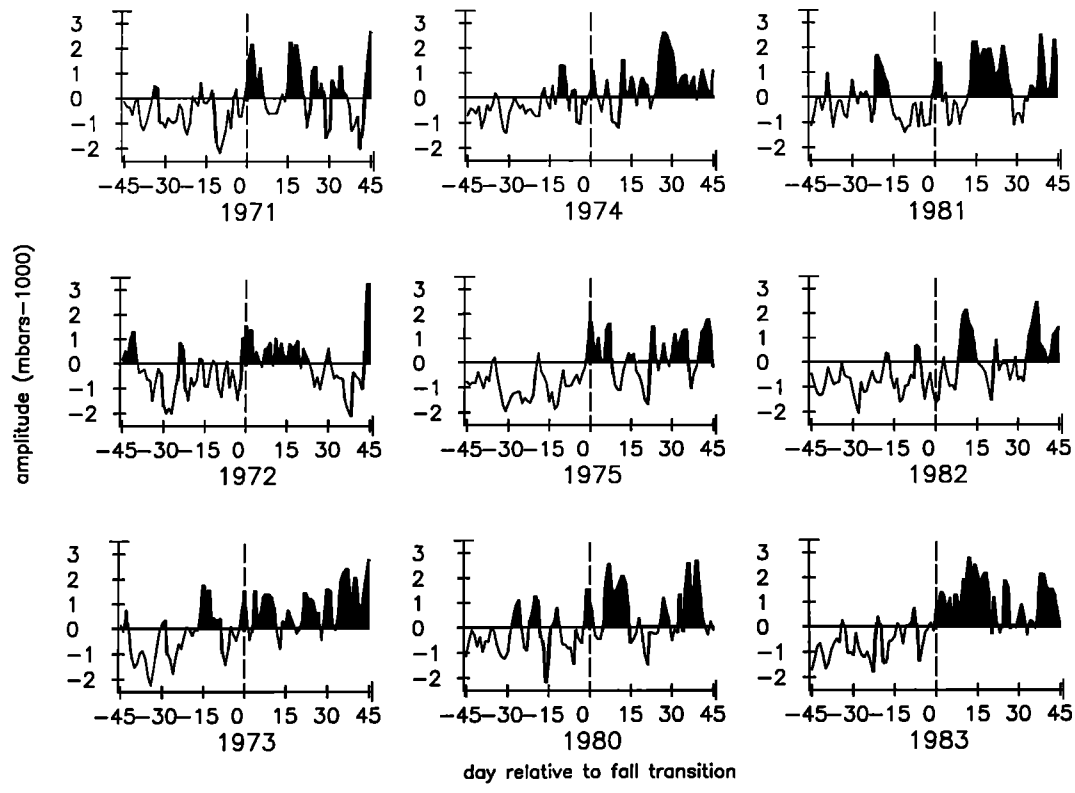

Fig. 18. Principal estimator pattern time series for the first SLP-ASL PEP for individual years. (*a*) For the spring transition, these correspond to the spatial patterns seen on the left of Figure 9*a*. (*b*) For the fall transition, these correspond to the spatial patterns seen on the left of Figure 14*a*.

Acknowledgments. We thank Steve Esbensen for his suggestions concerning atmospheric blocking, Dudley Chelton for referring us to the principal estimator patterns method, and John Horel for use of the 500-mbar data. Informal reviews by Ken Brink, Gad Levi, and two anonymous reviewers improved the manuscript. Some of the preliminary work was performed by Mike Dwyer, with support by the National Science Foundation's REU program (grant OCE-8712350). This work was supported in part by grant NAGW-869 from the National Aeronautics and Space administration and in part by contract N14-87-K-0242 from the Office of Naval Research.

REFERENCES

Breaker, L. C., and C. N. K. Mooers, Oceanic variability off the central California coast, *Prog. Oceanogr., 17*, 61–135, 1986.

Brink, K. H., D. W. Stewart, and J. C. Van Leer, Observations of the coastal upwelling region near 34°30'N off California: Spring 1981, *J. Phys. Oceanogr., 14*, 378–391, 1984.

Bryson, R. A., and J. F. Lahey, The march of seasons, *Rep. ASTIA AO-1525 00*, 41 pp., Dep. of Meteorol., Univ. of Wis., Madison, 1958.

Charney, J. G., J. Shukla, and K. C. Mo, Comparison of a barotropic blocking theory with observation, *J. Atmos. Sci., 38*, 762–779, 1981.

Davis, R. E., Techniques for statistical analysis and prediction of geophysical fluid systems, *Geophys. Astrophys. Fluid Dyn., 8*, 245–277, 1977.

Davis, R. E., Predictability of sea level pressure anomalies over the North Pacific Ocean, *J. Phys. Oceanogr., 8*, 233–246, 1978.

Dole, R. M., The life cycles of persistent anomalies and blocking over the North Pacific, *Adv. Geophys., 29*, 31–69, 1986.

Fleming, E. L., G.-H. Lim, and J. M. Wallace, Differences between the spring and atutumn circulation of the northern hemisphere, *J. Atmos. Sci., 44*, 1266–1286, 1987.

Graham, H. E., and W. B. White, The El Niño Cycle: A natural oscillator of the Pacific Ocean-atmosphere system, *Science, 240*, 1293–1302, 1988.

Haines, K., and J. Marshall, Eddy-forced coherent structures as a prototype of atmospheric blocking, *Q. J. R. Meteorol. Soc., 113*, 681–704, 1987.

Halliwell, G. R., and J. S. Allen, The large-scale coastal wind field along the west coast of North America, 1981–1982, *J. Geophys. Res., 92*, 1861–1884, 1987.

Hickey, B. M., The California current system–hypotheses and facts, *Prog. Oceanogr., 8*, 191–279, 1979.

Hickey, B. M., Patterns and processes of circulation over the continental shelf off Washington, in, *Coastal Dynamics of the Pacific Northwest*, edited by M. Landry and B. Hickey, Wiley-Interscience, New York, in press, 1989.

Hickey, B. M., and N. Pola, The seasonal alongshore pressure gradient on the west coast of the United States, *J. Geophys. Res., 88*, 7623–7633, 1983.

Horel, J. D., A rotated principal component analysis of the interannual variability of the northern hemisphere 500 mbar height field, *Mon. Weather Rev., 109*, 2080–2092, 1981.

Hotelling, H., Relations between two sets of variates, *Biometrika, 28*, 321–377, 1936.

Huyer, A. E., E. J. Sobey, and R. L. Smith, The spring transition in currents over the Oregon continental shelf, *J. Geophys. Res., 84*, 6995–7011, 1979.

Lahey, J. F., R. A. Bryson, and E. W. Wahl, *Atlas of Five-Day Normal Sea-Level Pressure Charts for the Northern Hemisphere*, University of Wisconsin Press, Madison, 1958.

Lanzante, J. R., Some singularities and irregularities in the seasonal progression of the 700 mbar height field, *J. Clim. Appl. Meteorol., 22*, 967–981, 1983.

Lentz, S., A description of the 1981 and 1982 spring transitions over the northern California shelf, *J. Geophys. Res., 92*, 1545–1567, 1987.

Malanotte-Rizzoli, P., and P. J. Hancock, Coherent structures in a baroclinic atmosphere, IV, A comparison between theory and data, *J. Atmos. Sci., 44*, 2506–2529, 1987.

Malanotte-Rizzoli, P., and P. Malguzzi, Coherent structures in a baroclinic atmosphere, III, Block formation and eddy forcing, *J. Atmos. Sci., 44*, 2493–2505, 1987.

McWilliams, J. C., An application of equivalent modons to atmospheric blocking, *Dyn. Atmos. Oceans, 5*, 43–66, 1980.

Mendenhall, B. R., M. M. Holl, and M. J. Cuming, Development of a marine history of analyzed sea-level pressure fields and diagnosed wind fields, *FNOC Tech. Rep. M-227*, 28 pp, Fleet Numer. Oceanogr. Cent., Monterey, Calif., 1977.

Mihok, W. F., and J. E. Kaitala, U.S. Navy fleet numerical weather central operational five-level global fourth-order primitive equation model, *Mon. Weather Rev., 12*, 1527–1550, 1976.

Nelson, C. S., Wind stress and wind stress curl over the California Current, *NMFS Rep. SSRF-714*, 87 pp., Natl. Oceanic and Atmos. Admin., Monterey, Calif., 1977.

Pierrehumbert, R. T., The effect of local baroclinic instability on zonal inhomogeneities of vorticity and temperature, *Adv. Geophys., 29*, 165–182, 1986.

Reid, B. J., The fall transition of Oregon waters, M.S. thesis, Coll. of Oceanogr., Oreg. State Univ., Corvallis, 1987.

Rex, D. F., Blocking action in the middle troposphere and its effects upon regional climate, I, An aerological study of blocking action, *Tellus, 2*, 196–211, 1950*a*.

Rex, D. F., Blocking action in the middle troposphere and its effects upon regional climate, II, The climatology of blocking action, *Tellus, 2*, 275–301, 1950*b*.

Richman, M. B., Rotation of principal components, *J. Climatol., 6*, 293–335, 1986.

Schutts, G. J., The propagation of eddies in diffluent jet streams: Eddy vorticity forcing of blocking flow fields, *Q. J. R. Meterol. Soc., 109*, 737–761, 1983.

Schutts, G. J., A case study of eddy forcing during an Atlantic blocking episode, *Adv. Geophys., 29*, 135–162, 1986.

Shukla, J., and K. C. Mo, Seasonal and geographical variation of blocking, *Mon. Weather Rev., 111*, 388–402, 1983.

Strub, P. T., J. S. Allen, A. Huyer, and R. L. Smith, Large-scale structure of the spring transition in the coastal ocean off western North America, *J. Geophys. Res., 92*, 1527–1544, 1987*a*.

Strub, P. T., J. S. Allen, A. Huyer, R. L. Smith, and R. C. Beardsley, Seasonal cycles of currents, temperatures, winds, and sea level over the northeast Pacific continental shelf: 35°N to 48°N, *J. Geophys. Res., 92*, 1507–1526, 1987*b*.

Werner, F. E., and B. M. Hickey, The role of a longshore pressure gradient in pacific northwest coastal dynamics, *J. Phys. Oceanogr., 13*, 395–410, 1983.

White, E. B., and N. E. Clark, On the development of locking ridge activity over the central North Pacific, *J. Atmos. Sci., 32*, 489–501, 1975.

Wickham, J. B., A. A. Bird, and C. N. K. Mooers, Mean and variable flow over the central California continental margin, *Continental Shelf Res., 7*, 827–849, 1987.

C. James and P. T. Strub, College of Oceanography, Oregon State University, Corvallis, OR 97331.

(Received June 30, 1988;
accepted August 12, 1988.)